UNSYMMETRIC LOADING OF A FRAMED DOME

by

SELWYN PERRIN FOX

B.A.Sc. (Forest Eng.)
University of British Columbia, 1952

M.A.Sc., University of Toronto, 1956

A THESIS SUBMITTED IN PARTIAL FULFILMENT OF

THE REQUIREMENTS FOR THE DEGREE OF

MASTER OF APPLIED SCIENCE

in the Department

of

CIVIL ENGINEERING

We accept this thesis as conforming to the
required standard

THE UNIVERSITY OF BRITISH COLUMBIA

May, 1967

In presenting this thesis in partial fulfilment of the requirements for an advanced degree at the University of British Columbia, I agree that the Library shall make it freely available for reference and study. I further agree that permission for extensive copying of this thesis for scholarly purposes may be granted by the Head of my Department or by his representatives. It is understood that copying or publication of this thesis for financial gain shall not be allowed without my written permission.

S. P. Fox

Department of Civil Engineering

The University of British Columbia
Vancouver 8, Canada

May, 1967

ABSTRACT

The linear analysis of a specific framed dome is mapped for the unsymmetric loadings of half snow and wind. The joints of the dome, to which the loads are applied, lie on a spherical surface but the connecting members are straight.

Several parameters, such as the perimeter ring size, the web member area, geometric conformity, and joint fixity, are changed and the effects of these changes are compared and discussed.

It is shown that membrane shell theory closely approximates the member forces induced by wind. An approximate system to find the member forces is presented and compared with the exact analysis. This system is based on overall structure equilibrium and an assumed distribution of edge shear.

All analyses were made using a space frame program based on the stiffness method with six degrees of freedom per joint. An IBM 7040 computer was used for calculations.

TABLE OF CONTENTS

	Page
TABLE OF CONTENTS	i
LIST OF TABLES	iii
LIST OF FIGURES	iv
NOTATION	vi
ACKNOWLEDGEMENTS	viii
CHAPTER	
I INTRODUCTION	1
II THE STANDARD DOME	
2.1 Description	3
2.2 Applied and Internal Forces	5
2.3 Rib and Web Force Distributions	
2.3.1 Conventions	5
2.3.2 Half-Snow Loading	8
2.3.3 Wind Loading	8
2.4 Perimeter Ring Forces	23
2.5 Displacements of the Standard Dome	23
2.6 Stress Analysis of the Web Members and Rib	
2.6.1 Criteria	25
2.6.2 Live Load Stress Analysis	25
III EFFECT OF PARAMETER VARIATION	
3.1 Introduction	27
3.2 Variation of the Perimeter Ring Size	
3.2.1 Properties of the Domes PR1 and PR2	27
3.2.2 General Effect on Web and Rib Forces	28
3.2.3 Change in Stresses	28
3.2.4 Change in Displacements	38
3.2.5 Change in Perimeter Ring Forces	38

TABLE OF CONTENTS (Continued)

		Page
	3.3 Web Member Area Reduction	
	3.3.1 Properties of the Dome A/3	40
	3.3.2 General Effect on Web and Rib Forces	40
	3.3.3 Change in Stresses	40
	3.3.4 Change in Displacements	41
	3.4 Change in Member End Condition	
	3.4.1 The Pinned-End Condition	41
	3.4.2 The Fixed-End Condition	42
	3.5 A Local Geometry Change	43
IV	APPROXIMATING THE MAXIMUM DIAGONAL FORCE	
	4.1 Past Work	46
	4.2 Half-Snow Loading	47
	4.3 Wind Loading	
	4.3.1 Shell Analogy	55
	4.3.2 Freebody Approach	57
V	CONCLUSIONS	60
LIST OF REFERENCES		62
APPENDIX		63

LIST OF TABLES

Table		Page
1	Maximum Internal Force Comparison (Half Snow)	9
2	Eccentricity of the Force F_ϕ (Half Snow)	9
3	Maximum Internal Force Comparison (Wind)	22
4	Eccentricity of the Force F_ϕ (Wind)	23
5	Perimeter Ring Forces of the Standard Dome	24
6	Significant Properties of the Perimeter Rings	37
7	Ratios of Rib Forces for Full-Snow Loading	38
8	Ratios of Maximum Displacements of 'PR1' and 'PR2' Perimeter and Lantern Rings Compared to 'STD'	39
9	Ratios of Maximum Displacements of 'PR1' and 'PR2' Compared to 'STD', at about $\phi = 17^\circ$	39
10	Perimeter Ring Stress Comparison, Psi	39
11	Calculation of V for Half-Snow Loading	51
12	Comparison of Maximum Diagonal Forces (Kips) at $\theta = 97.5^\circ$ for Half-Snow Loading	56
13	Calculation of V for Wind Loading at $\phi = 31^\circ$	56

LIST OF FIGURES

Figure		Page
1	The Standard Dome "STD"	4
2	Loading Systems	6
3	Forces Computed by the Analysis	6
4	Six Selected Forces	7
5	Diagonal Force Definition	7
6	F_ϕ (Kips) Half Snow	10
7	V_ϕ (Kips) Half Snow	11
8	M_ϕ (Ft-Kips) Half Snow	12
9	F_θ (Kips) Half Snow	13
10	$F^+_{\phi\theta}$ (Kips) Half Snow	14
11	$F^-_{\phi\theta}$ (Kips) Half Snow	15
12	F_ϕ (Kips) Wind	16
13	V_ϕ (Kips) Wind	17
14	M_ϕ (Ft-Kips) Wind	18
15	F_θ (Kips) Wind	19
16	$F^+_{\phi\theta}$ (Kips) Wind	20
17	$F^-_{\phi\theta}$ (Kips) Wind	21
18	Maximum Compressive F_ϕ Half Snow	29
19	Maximum V_ϕ Half Snow	30
20	Maximum (Absolute) M_ϕ Half Snow	31
21	Maximum F_θ Half Snow	32
22	Maximum Compressive $F_{\phi\theta}$	33
23	Maximum F_ϕ Wind	34

LIST OF FIGURES (Continued)

		Page
24	Maximum V_ϕ Wind	35
25	Maximum M_ϕ Wind	36
26	Maximum F_θ Wind	37
27	Special Geometry of the Dome 'GEO'	45
28	Freebody for Unsymmetric Loading	49
29	Freebody for Half Snow	49
30	V Distributions for Half Snow	52
31	Calculation of Exact V	53
32	V Distributions for Wind	53
33	Freebody for Wind	58

NOTATION

A	Cross-sectional area of a member
E	Modulus of elasticity
F	Axial force
F_a , F_c	Allowable axial stresses
F_b	Allowable bending stress
F_v	Allowable shear stress
G	Shear modulus of elasticity
H	Resultant of the shear flow
H.S.	Half-snow loading
I_x , I_y	Moment of inertia about the x-x or y-y axis
J	Polar moment of inertia
K	Structure stiffness matrix or function of E and F_c
L, L^T	Lower triangular matrix and its transpose
L	Live load
M	Bending moment at a joint
$N\phi\theta$	Shear force of membrane shell theory
P	Resultant of the half-snow loading
Q	Resultant of the wind loading
S	Section modulus
T	Horizontal component of Q
U.D.L.	Full-snow loading (uniformly distributed loading)
V	Transverse shear force or edge shear flow
V_o	Maximum shear flow

NOTATION (Continued)

a	Spherical radius
b	Breadth of member or lever arm
d	Depth of member or lever arm
e	Eccentricity or lever arm
f_a	Actual axial stress, F/A
f_b	Extreme fibre stress in bending, M/S
f_v	Actual shear stress
i	Counting index
ℓ	Effective column buckling length
m	Lever arm
n	Joint number counting from the lantern ring toward the perimeter ring
p_o	Wind pressure at $\phi = 90^o$
r	Radius
s	Approximate distance
ΔH	Maximum horizontal displacement ratio
ΔMAX	Maximum total translation ratio
ΔV	Maximum vertical displacement ratio
α	Angle between one of the principal axes of the member and the plane which passes through the member's axis and is also perpendicular to the XZ plane of the dome
α_n	Angle between a rib segment and the XZ plane
β_n	Angle between a rib segment and the diagonal
η	Ratio of f_b/f_a
θ, ϕ	Spherical coordinates
λ	Angle between a diagonal and the ring member

ACKNOWLEDGEMENTS

The author wishes to express his appreciation for the encouragement received from his supervisor, Dr. R. F. Hooley, during residence studies and also for his guidance during the preparation of this thesis.

The author is grateful to the National Research Council of Canada and to the University of British Columbia for financial assistance during two winters of study.

The opportunity is taken here, as well, to acknowledge the essential support received from his wife, Barbara, during the period of study and discipline.

May, 1967

Port Coquitlam, B. C.

UNSYMMETRIC LOADING OF A FRAMED DOME

CHAPTER I

INTRODUCTION

One common method to cover large areas is to construct a dome either as a space frame or truss rather than as a continuous shell. Some notable examples are the Schwedler Dome of Berlin, the Dome of Discovery of London, the R. Buckminster Fuller geodesic domes and the Astrodome of Houston, Texas. Much information exists for the analysis of such structures for axi-symmetric loads if the members are pin-ended. A designer finds little information on the behaviour of such structures subjected to unsymmetric loads.

An objective of this thesis is to provide the designer with the exact linear response of one such dome carrying unsymmetric loads and to show how the behaviour changes when various design parameters are altered. Chapters II and III present these analyses as a report of assorted factual information to aid the designer of geometrically similar framed domes. With this information, the order of magnitude of internal forces, stresses, and deflections of a similar dome can be estimated through the laws of models. The effects of each unsymmetric loading are considered separately and compared often to the effects of a uniformly distributed loading over the vertical projection of the dome. No attempt has been made to determine the effects of a superposition of loadings.

Another objective of this thesis is to present approximate systems of calculation to aid the designer in his choice of preliminary sizes. An approximation to the exact response of the diagonals is given for each unsymmetric loading.

The non-linear analysis or buckling of these mesh domes, although more important than the response to unsymmetric loads, is left to a later study.

The dome chosen for study is shown in Fig. 1. The joints lie on a spherical surface but the members are straight. This structure, as illustrated, will be referred to as the standard dome, STD, and the distribution of six forces will be given for a wind loading and for a uniform snow loading over one half the dome.

Later chapters will show, in turn, how the response of this standard dome varies due to:

(a) a change in the bending and axial stiffness of the perimeter ring,

(b) a reduction, by two-thirds, of the area of the web members,

(c) changing groups of members from pinned ends to fixed ends,

(d) an imperfection in the joint geometry owing to a possible fabrication error, and

(e) the rate of change of snow depth from the unloaded region to the uniformly loaded region.

For all variations of the dome and its loadings, an exact analysis was made by the stiffness method, using six degrees of freedom per joint, an IBM 7040 computer, and treating the dome as a space structure.

CHAPTER II

THE STANDARD DOME

2.1 Description

The geometric and elastic properties of the standard dome are shown in Fig. 1. The angle, α, is the inclination of one of the principal axes of the member cross-section to a plane through the member's axis and perpendicular to the XZ plane. The timber sizes were considered to be reasonable for the forces applied to the standard dome. A stress analysis at the end of this chapter shows that the timber members chosen were stressed within their allowable stresses for the assumed buckling conditions. The response of this dome made of other materials would be the same if the distribution of AE and EI was identical.

In the standard dome, there are five principal members: the perimeter ring, the lantern ring, the ribs, the intermediate rings and the diagonals. The latter two members help to brace the rib and will be called 'web members' since they are analogous in function to the web of a truss.

The perimeter ring, lantern ring, and the ribs were continuous members: each segment was fixed to the next. The ribs were fixed to the lantern ring but were pinned to the perimeter ring. The web members were pinned to the ribs. Anchorage of the dome was provided by a simple system of pinned-end columns and double diagonal bracing which supported the dome at each junction of a rib and the perimeter ring. These columns were 26.67 ft in length by 300.0 $in.^2$ in area. The diagonals were 150.0 $in.^2$ in area.

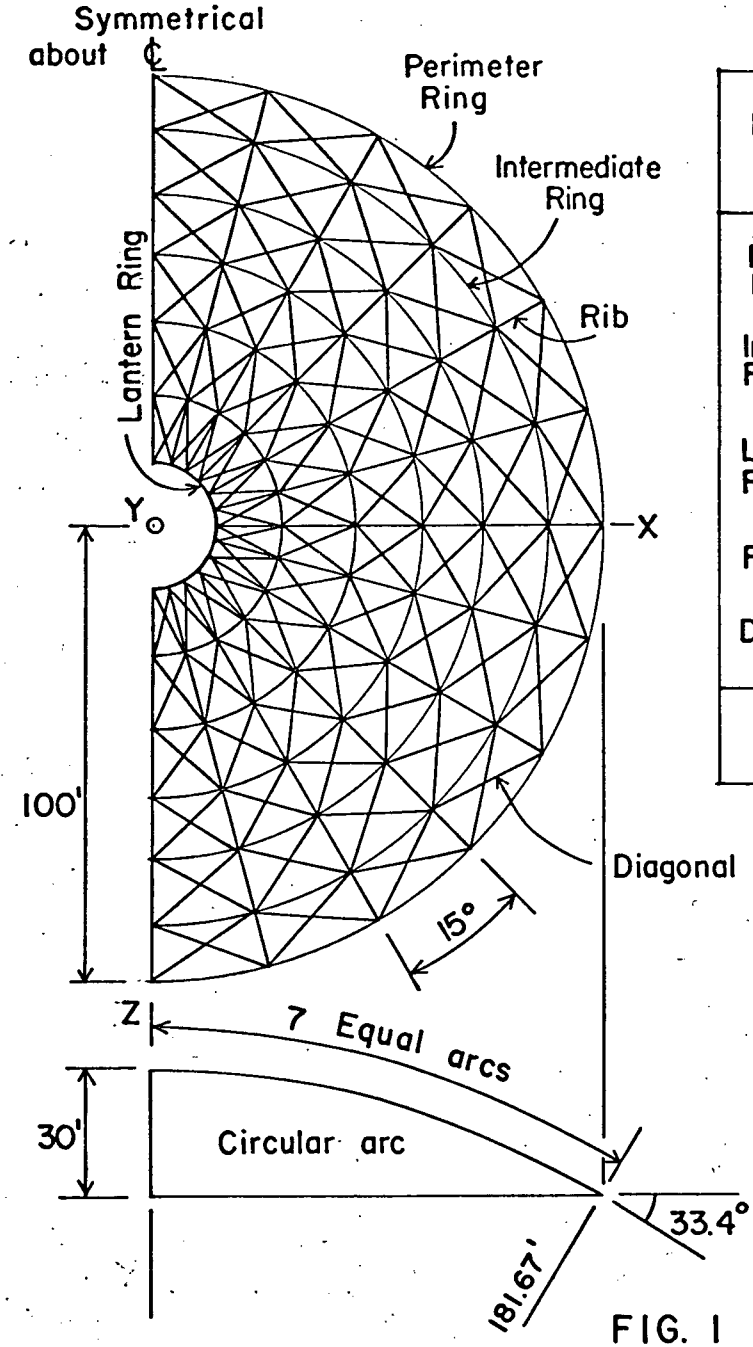

Member	Size in	A in^2	I_x in^4	I_y in^4	J in^4	α deg.
Perimeter Ring	60x18	1080	29,160	324,000	94,500	0
Intermediate Rings	5x10	50	415	105	285	Varies
Lantern Ring	10x10	100	833	833	1,400	0
Rib	5x30	150	11,250	310	1,120	0
Diagonal	5x15	75	1,405	155	495	Varies
E = 2000 ksi , G = 120 ksi , Timber						

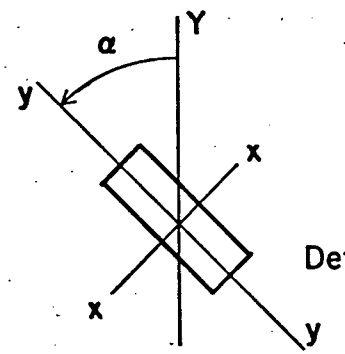

Definition of α

FIG. 1 THE STANDARD DOME "STD"

2.2 Applied and Internal Forces

The two unsymmetric loadings applied to the dome are shown in Fig. 2. These distributed loadings were concentrated at each joint according to the pressure at and the surface area tributary to the joint. According to the member end condition, the force analysis provided the internal forces shown in Fig. 3. An examination of these forces computed for the standard dome indicated that the following six forces shown in Fig. 4 might govern design and so were chosen for study:

(a) the axial force in each rib segment, F_ϕ,

(b) the rib bending moment about the strong axis at each joint, M_ϕ,

(c) the rib shear normal to the strong axis of each rib segment, V_ϕ,

(d) the axial force in each web ring member, F_θ, and

(e) the axial force in each diagonal member, $F_{\phi\theta}^{+}$ or $F_{\phi\theta}^{-}$, the superscripts referring to the slope of the diagonal as defined by the coordinates ϕ and θ (Fig. 5).

A more detailed examination of the other forces in the analysis is left for a later study.

2.3 Rib and Web Force Distributions

2.3.1 Conventions

The distributions of the six selected forces have been mapped as shown in Figs. 6 to 17 according to the sign convention defined by Fig. 4 and the applied loadings of Fig. 2.

To plot an equal force line, one assumption was necessary: a force which is constant in magnitude throughout the member length was assumed to act at the mid-length of that member. The plot of the bending moment, M_ϕ, is an exception to this rule since the method of analysis calculates the value of M_ϕ for a discrete point which is the rib joint.

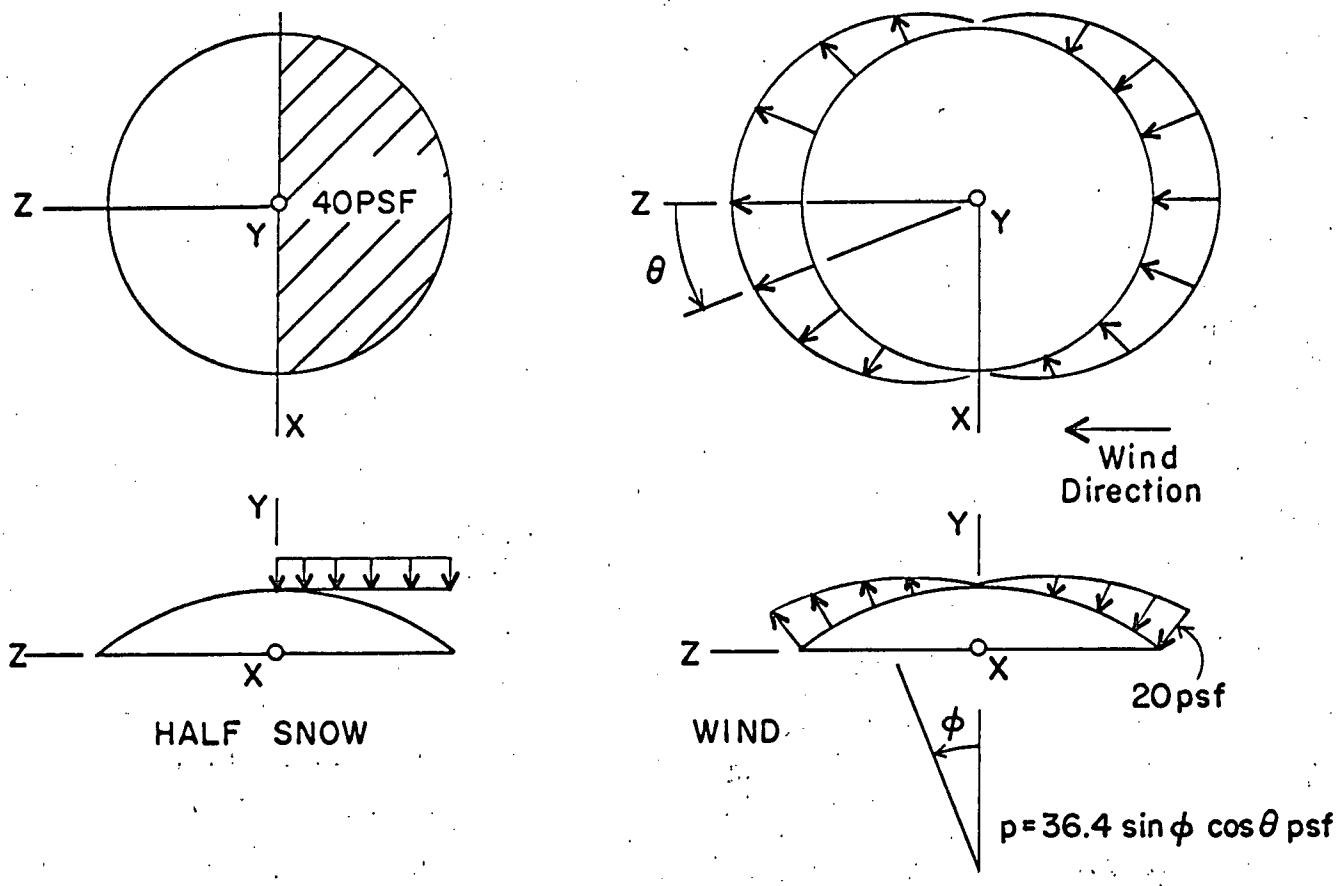

FIG. 2 LOADING SYSTEMS

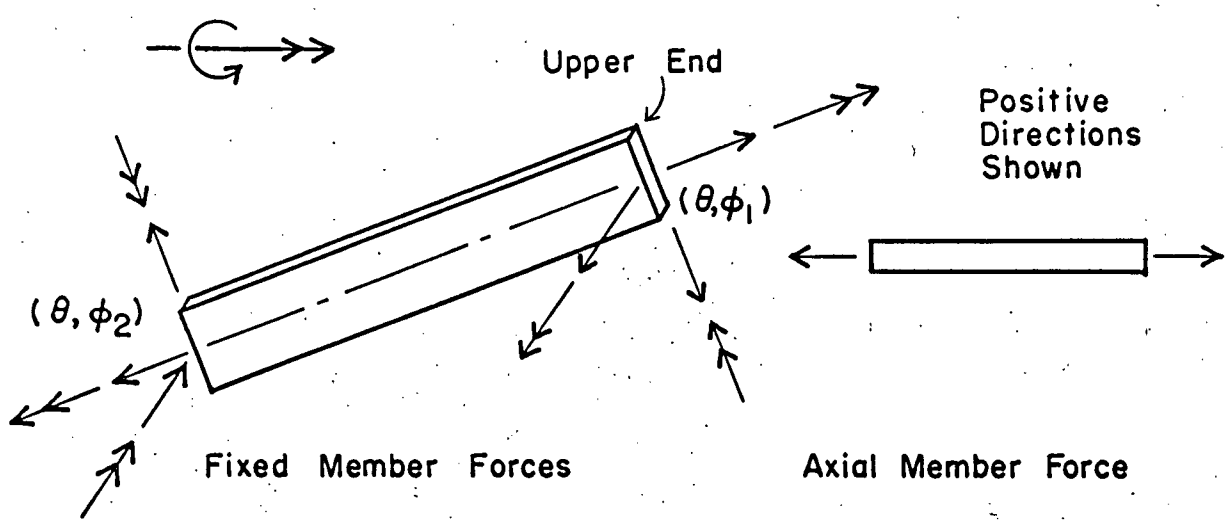

FIG. 3 FORCES COMPUTED BY THE ANALYSIS

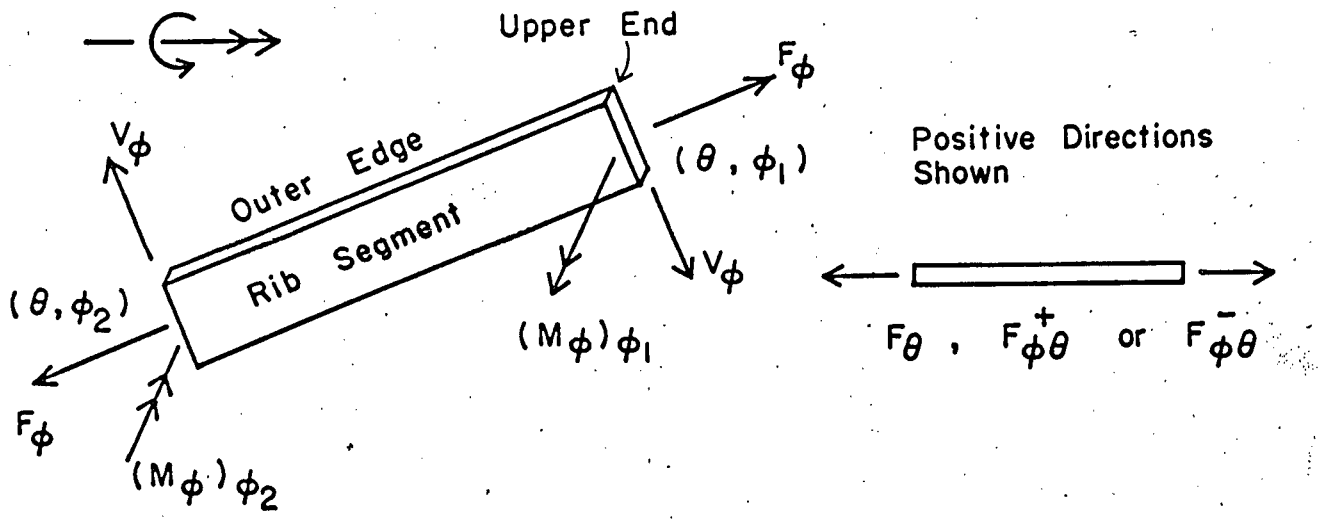

FIG. 4 SIX SELECTED FORCES

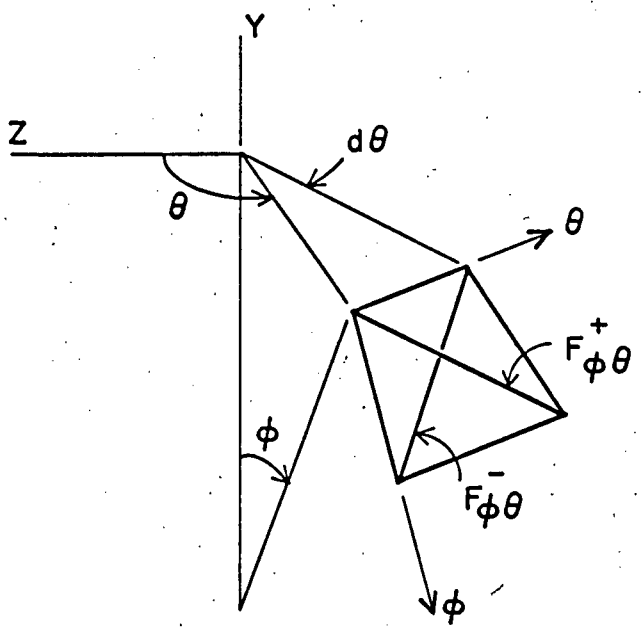

FIG. 5 DIAGONAL FORCE DEFINITION

2.3.2 Half-Snow Loading

A consideration of Figs. 6 to 11 will show that the extreme values of the forces in the rib segments and the diagonals are found near the transition of the snow load. In this same vicinity, the force of the web rings has a change in sign. Furthermore, these extreme rib and diagonal forces occur near the perimeter ring, whereas the maximum web ring force is found near the lantern ring.

The half-snow loading has a significant effect on the internal forces. Table 1 compares maximum forces created by half snow with forces created by full snow; that is, a covering of the entire dome with a uniformly distributed load of 40 psf. The half-snow values (H.S.) are expressed as a percentage of the full-snow values (U.D.L.).

The rib bending moment, M_ϕ, can be considered to be caused by an eccentricity, e, of the axial force, F_ϕ, expressed by $M_\phi = F_\phi e$, or the bending can be discussed as the ratio, η, of the bending stress, f_b, and the axial stress, f_a, where

$$\eta = \frac{f_b}{f_a} = \frac{6M_\phi}{bd^2} \Big/ \frac{F_\phi}{bd} = \frac{6e}{d}$$

Table 2 shows e as well as η for the worst stressed 30.0 in. rib depth of the standard dome ($\theta = 105^\circ$). Similar values for the standard dome covered with full snow are shown for comparison.

These bending stresses are comparable to the secondary stresses induced in a rigid-jointed plane truss because of joint deflection. In normal truss design these secondary stresses are neglected unless the members are stubby. Whether they should be neglected in the framed dome where the ratio, η, is much higher than in a plane truss is a matter for further study.

2.3.3 Wind Loading

The wind load applied to the dome represents a pressure action on the windward half and a suction action on the leeward. The pressure distribution was taken as $36.4 \sin \phi \cos \theta$ which approximates a 120 mph wind

and creates 20 psf at the perimeter ring on each side of the dome (Fig. 2). Force distributions shown in Figs. 12 to 17 reflect the anti-symmetrical nature of wind load.

TABLE 1. MAXIMUM INTERNAL FORCE COMPARISON (HALF SNOW)

ϕ degrees		31	26	21	17	12	7
F_ϕ kips	H.S.	-67.2	-53.0	-43.0	-31.8	-20.7	-9.2
	U.D.L.	-82.3	-58.0	-36.5	-20.1	-10.5	-6.7
	%	81.7	91.4	118	158	197	137
V_ϕ kips	H.S.	1.26	-0.64	-0.35	0.17	-0.14	-0.44
	U.D.L.	0.91	-0.49	-0.11	0.15	-0.08	-0.39
	%	138	130	318	113	175	113
$F_{\phi\theta}$ kips	H.S.	-34.3	-39.9	-37.0	-34.2	-28.5	-25.7
	U.D.L.	-5.18	-16.7	-20.6	-19.5	-15.1	-9.56
	%	662	239	180	175	189	269
ϕ degrees		28.6	23.9	19.1	14.3	9.5	4.8
M_ϕ ft-kips	H.S.	19.1	9.45	4.95	7.46	5.85	-2.11
	U.D.L.	13.8	6.40	4.70	6.89	5.75	-0.20
	%	138	148	105	108	102	1055
F_θ kips	H.S.	-6.54	-18.3	-27.2	-35.7	-44.3	--
	U.D.L.	-1.94	-11.6	-18.1	-23.6	-29.1	--
	%	337	158	150	151	152	--

Note: For half-snow loading (H.S.) and any given ϕ, the values F_ϕ, V_ϕ, and M_ϕ shown do not necessarily occur in the same member.

TABLE 2. ECCENTRICITY OF THE FORCE F_ϕ (HALF SNOW)

ϕ degrees	Half Snow e in.	Half Snow η	Full Snow e in.	Full Snow η
28.6	3.7	0.74	2.0	0.40
23.9	2.1	.43	1.3	.26
19.1	1.1	.23	1.6	.31
14.3	1.7	.34	4.1	.82
9.5	3.3	.65	6.6	1.32
4.8	1.7	.34	0.4	0.07

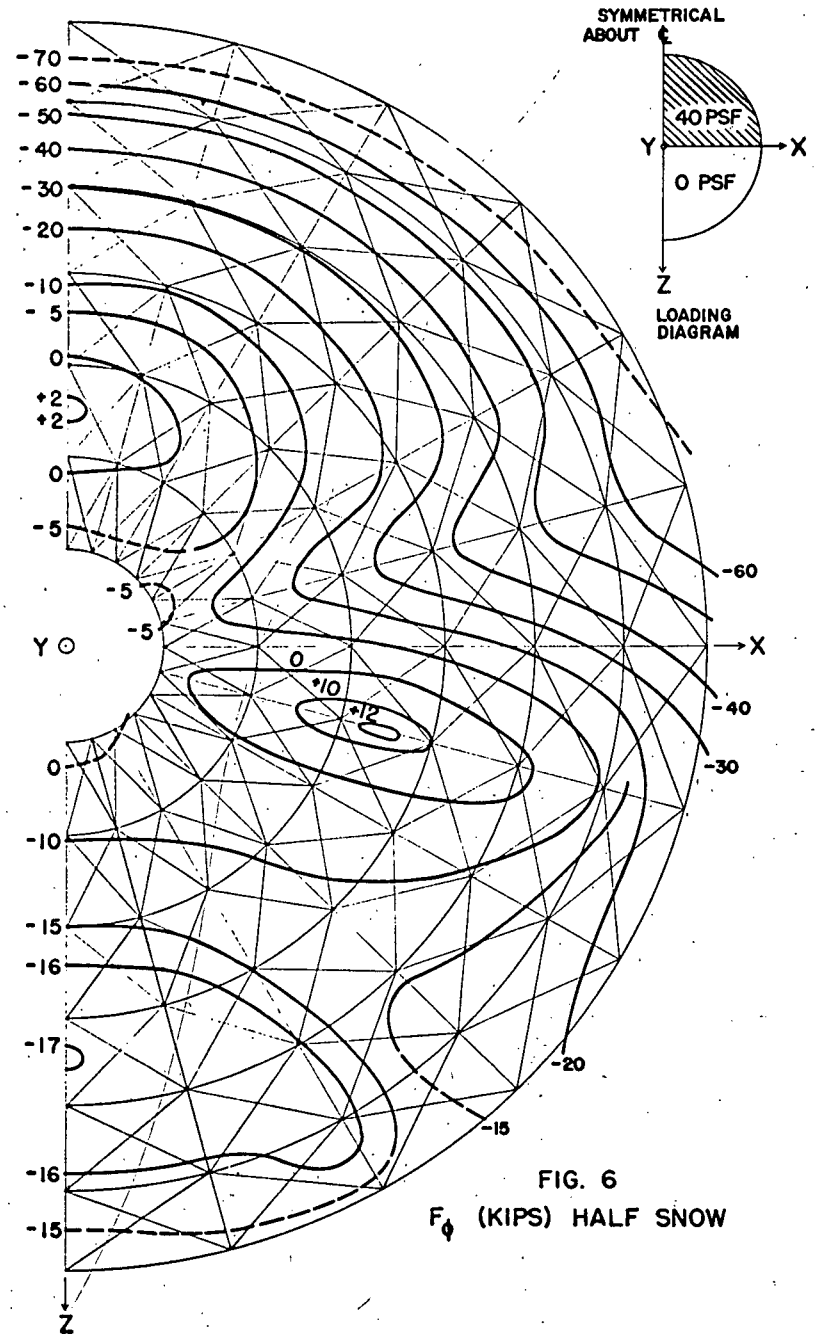

FIG. 6
F_ϕ (KIPS) HALF SNOW

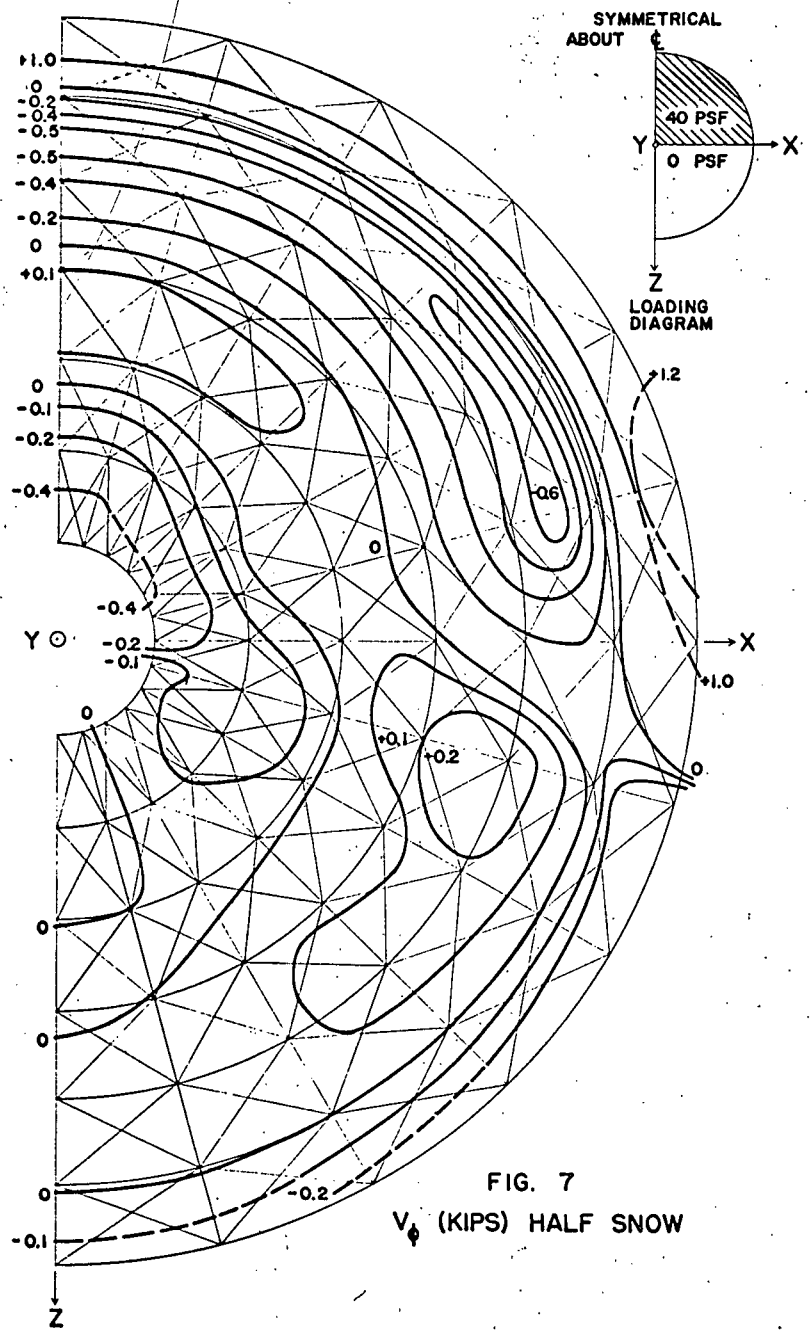

FIG. 7

V_ϕ (KIPS) HALF SNOW

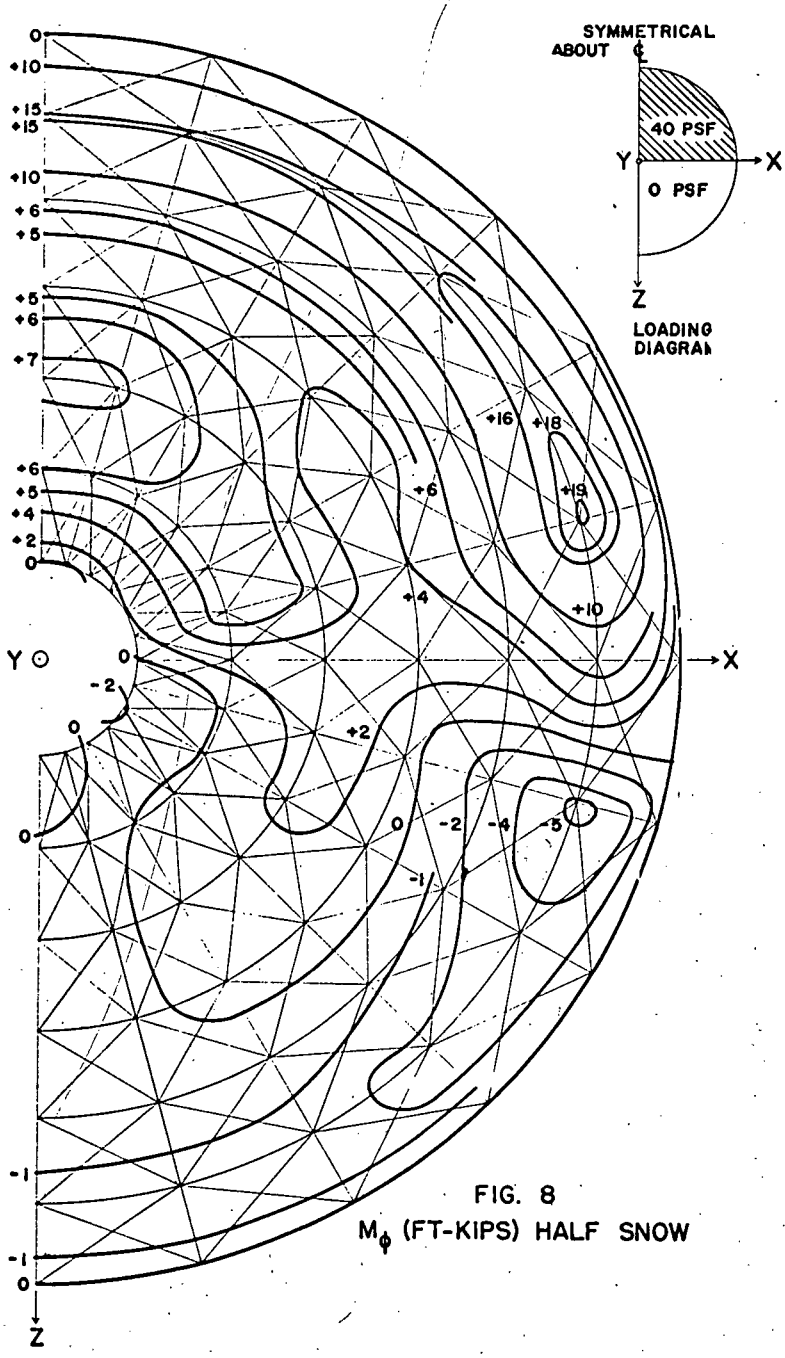

FIG. 8
M_ϕ (FT-KIPS) HALF SNOW

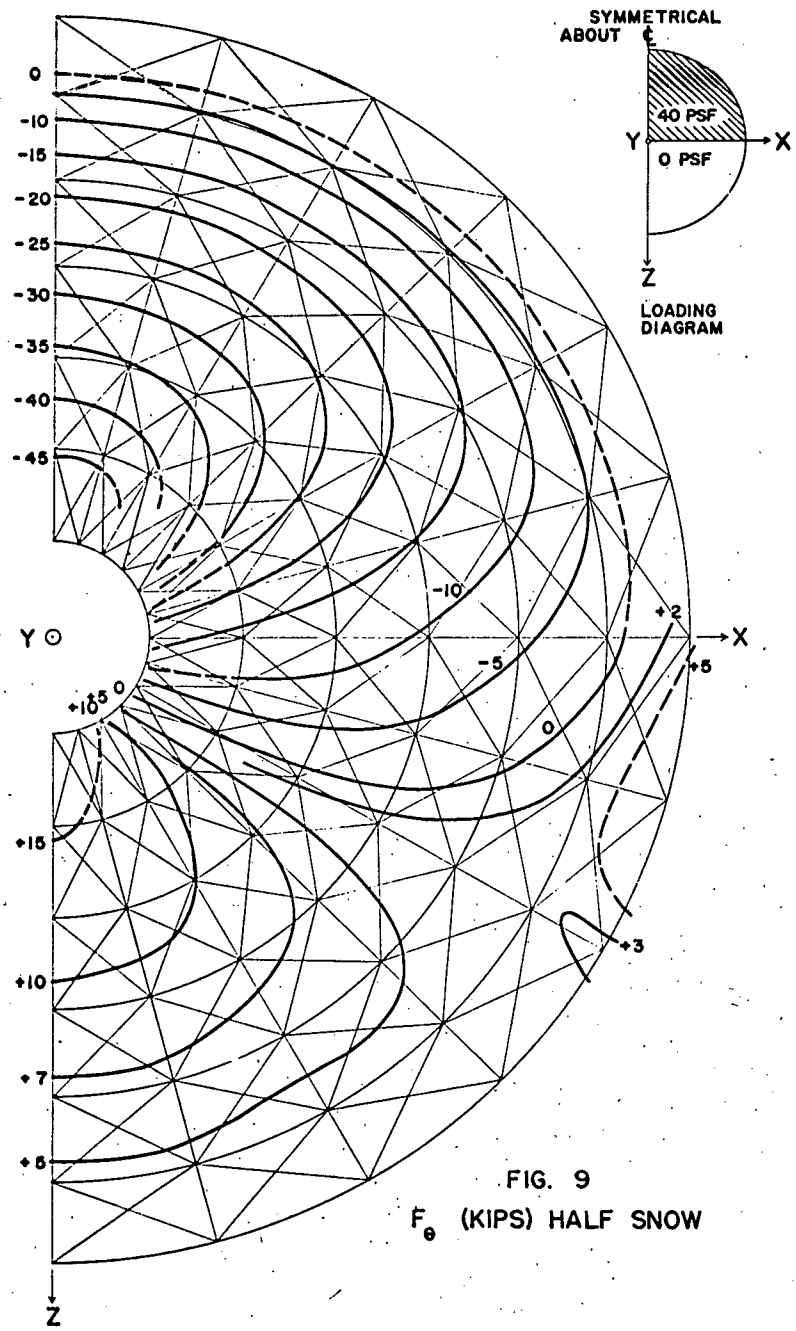

FIG. 9

F_θ (KIPS) HALF SNOW

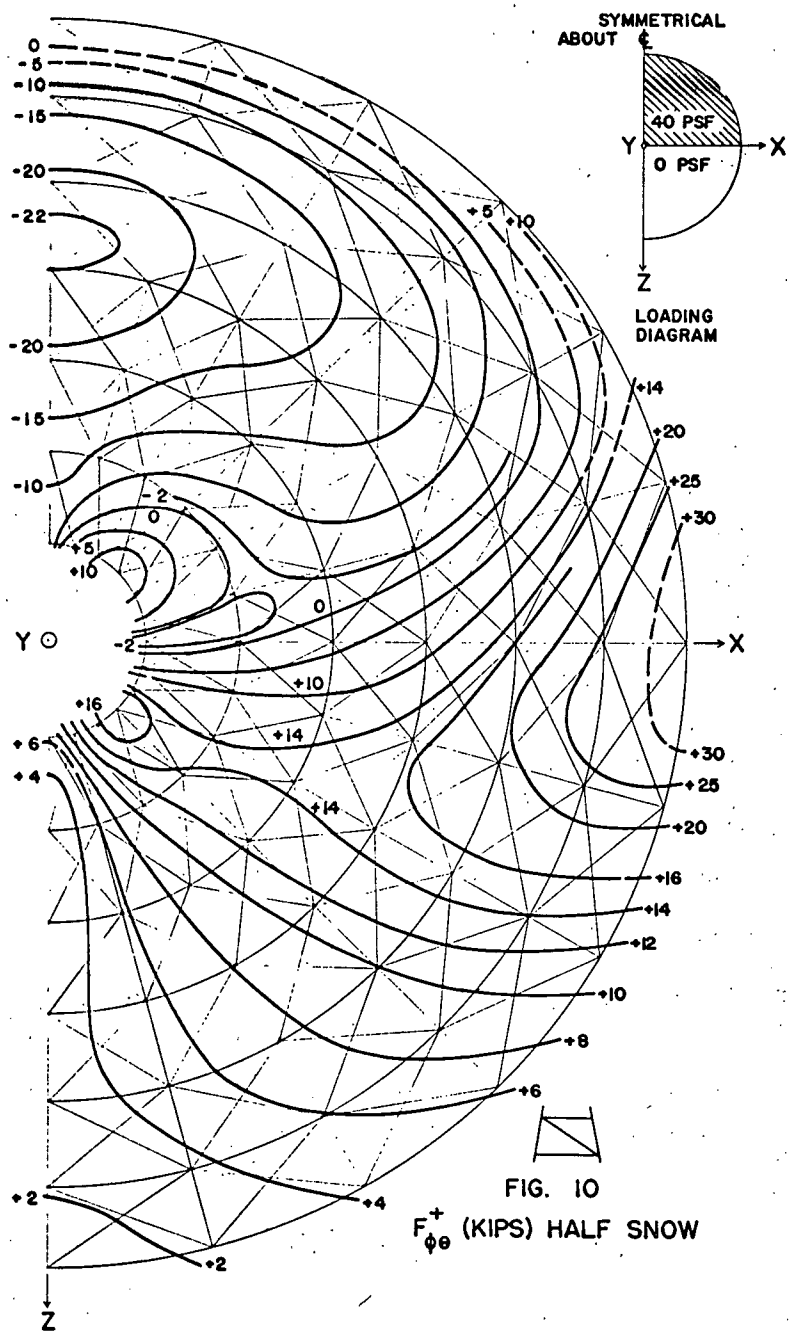

FIG. 10

$F^{+}_{\phi\theta}$ (KIPS) HALF SNOW

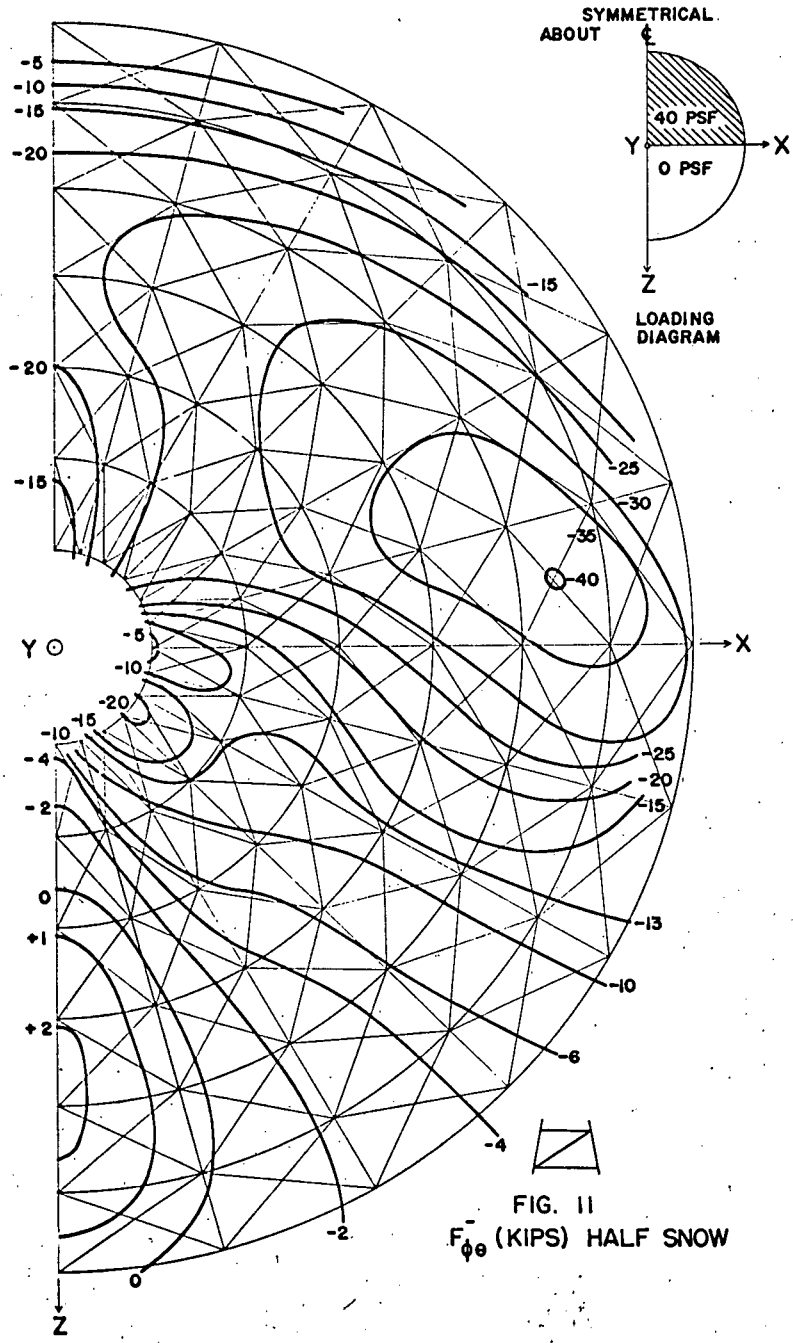

FIG. 11
$F_{\phi\theta}^{-}$ (KIPS) HALF SNOW

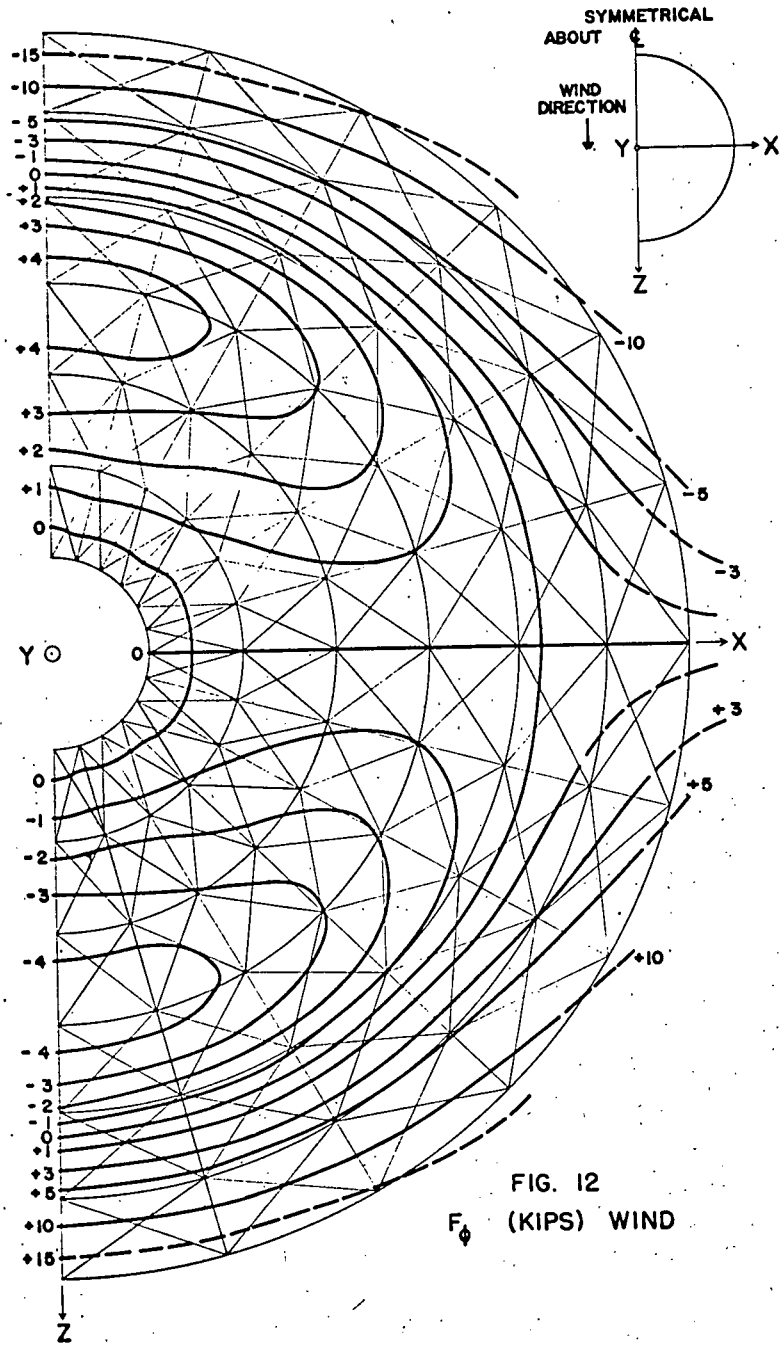

FIG. 12

F_ϕ (KIPS) WIND

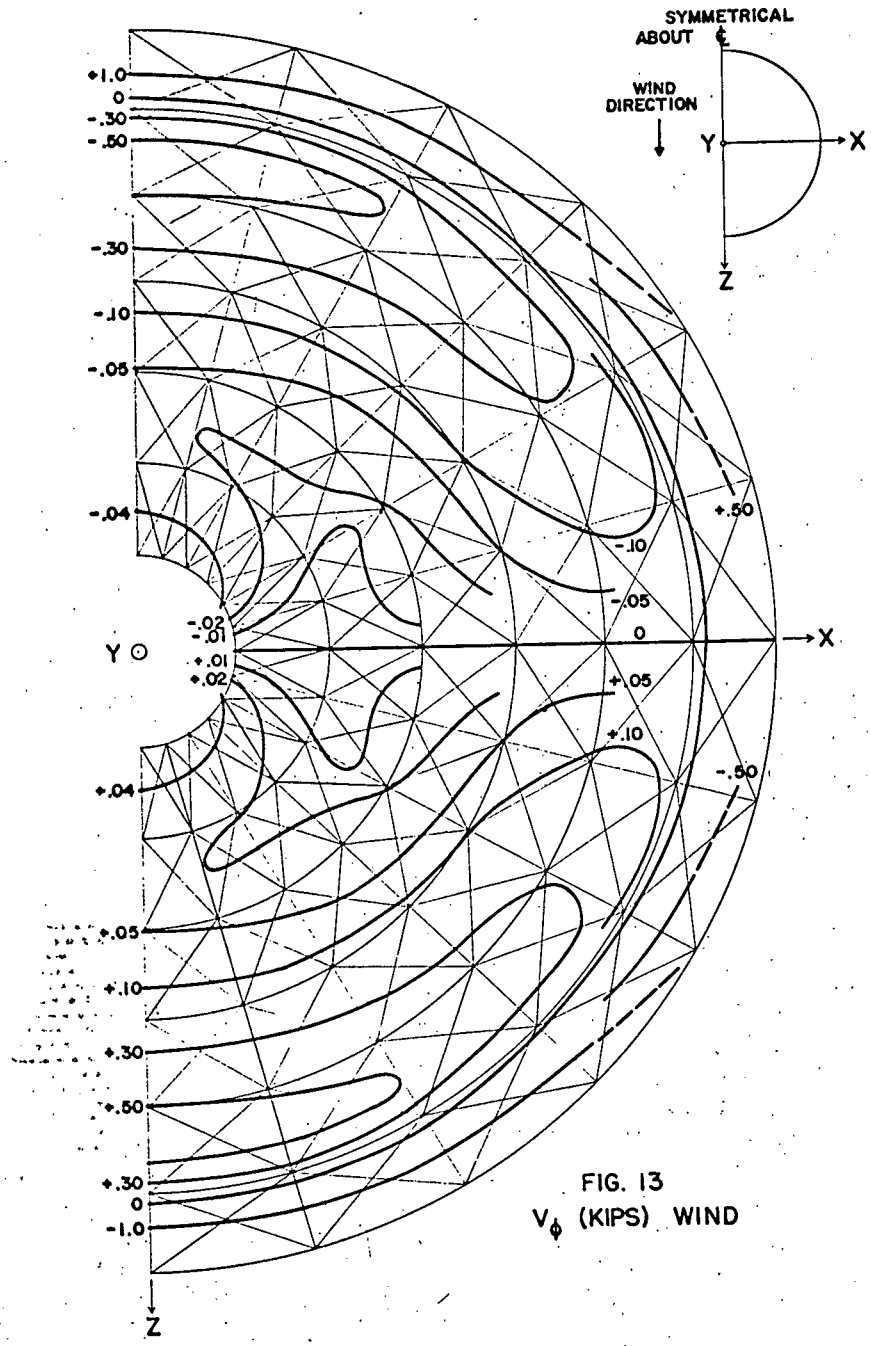

FIG. 13
V_ϕ (KIPS) WIND

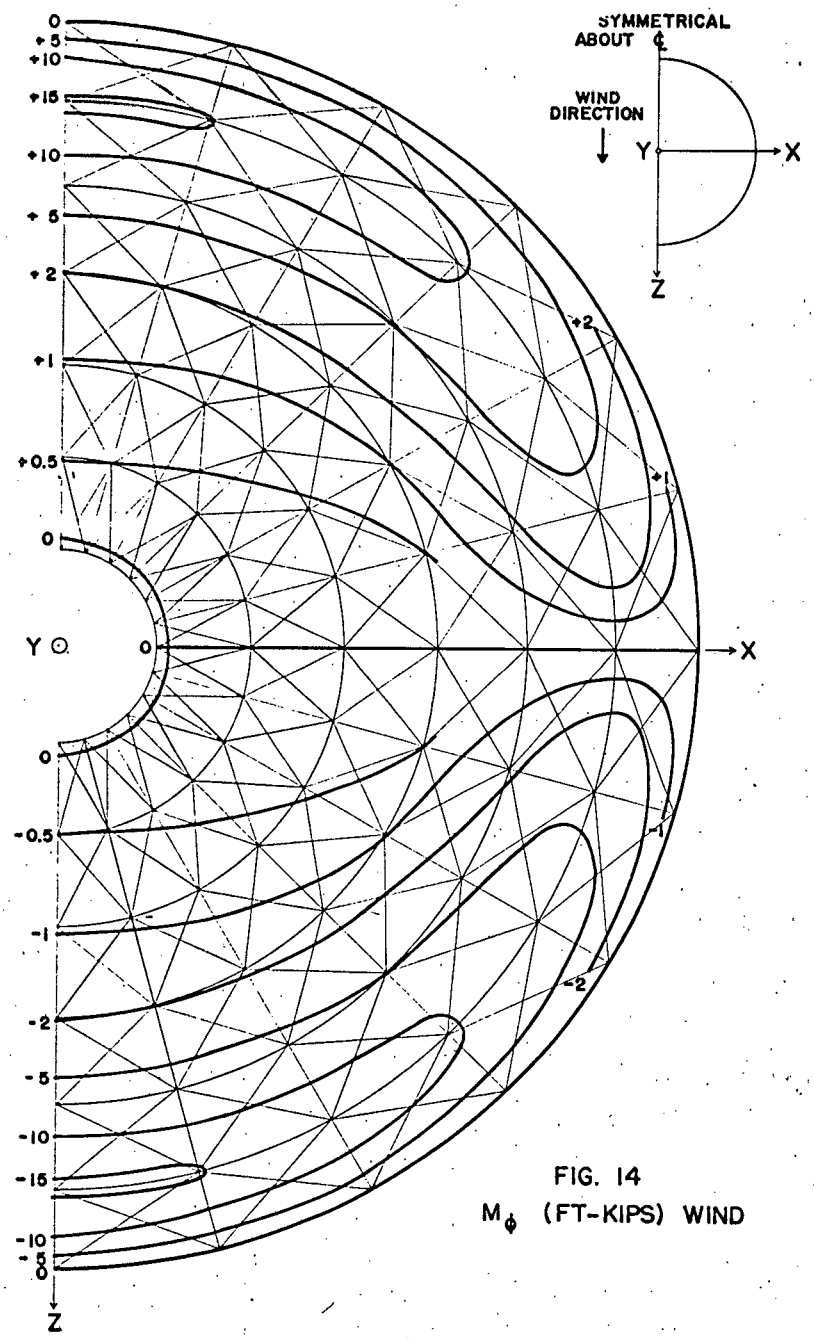

FIG. 14
M_ϕ (FT-KIPS) WIND

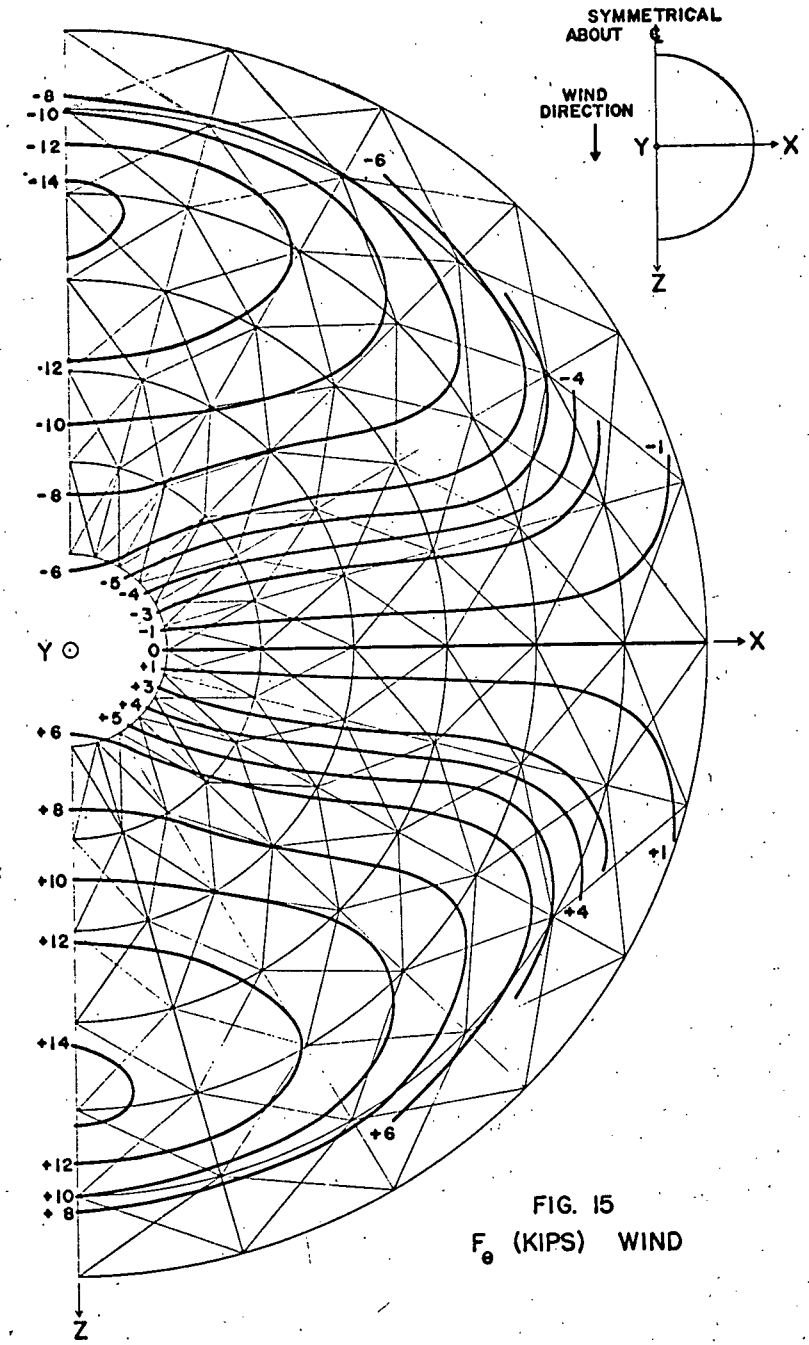

FIG. 15
F_θ (KIPS) WIND

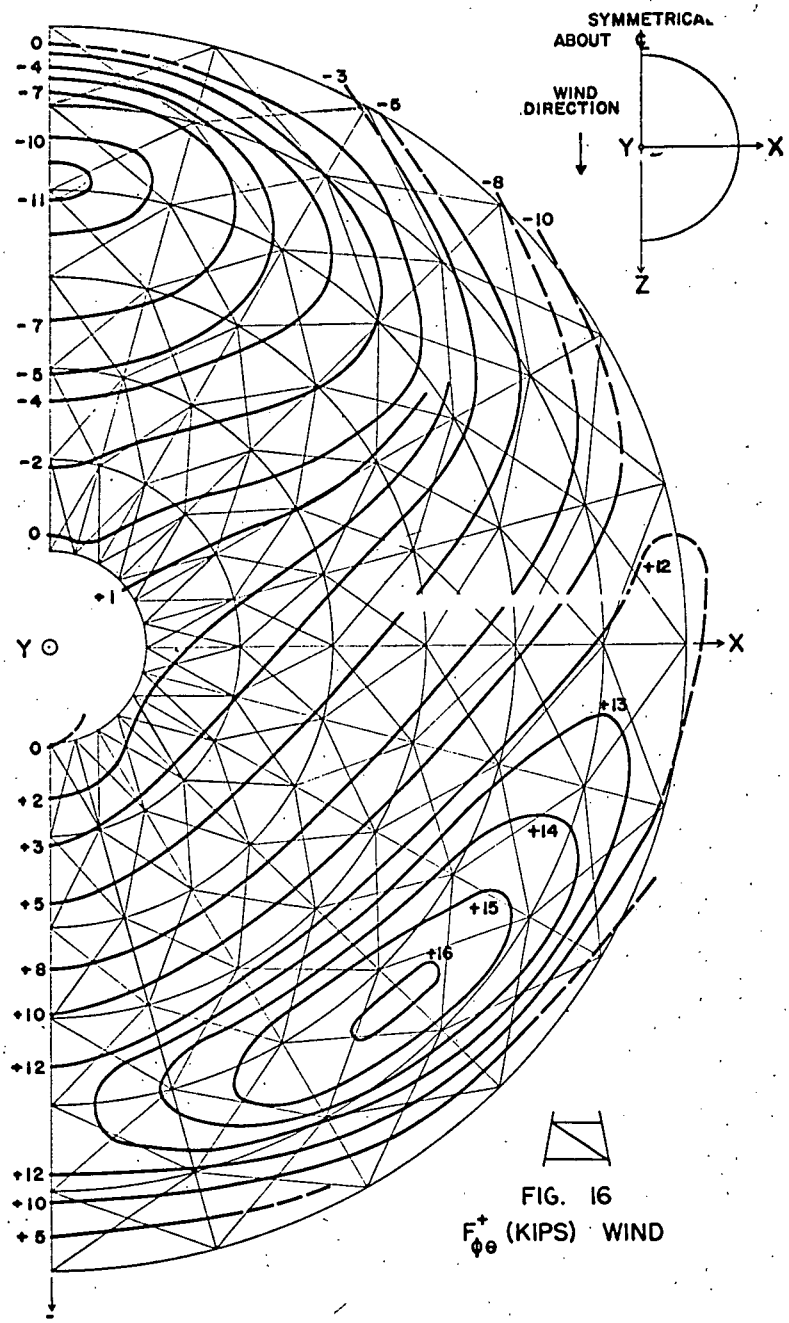

FIG. 16
$F^{+}_{\phi\theta}$ (KIPS) WIND

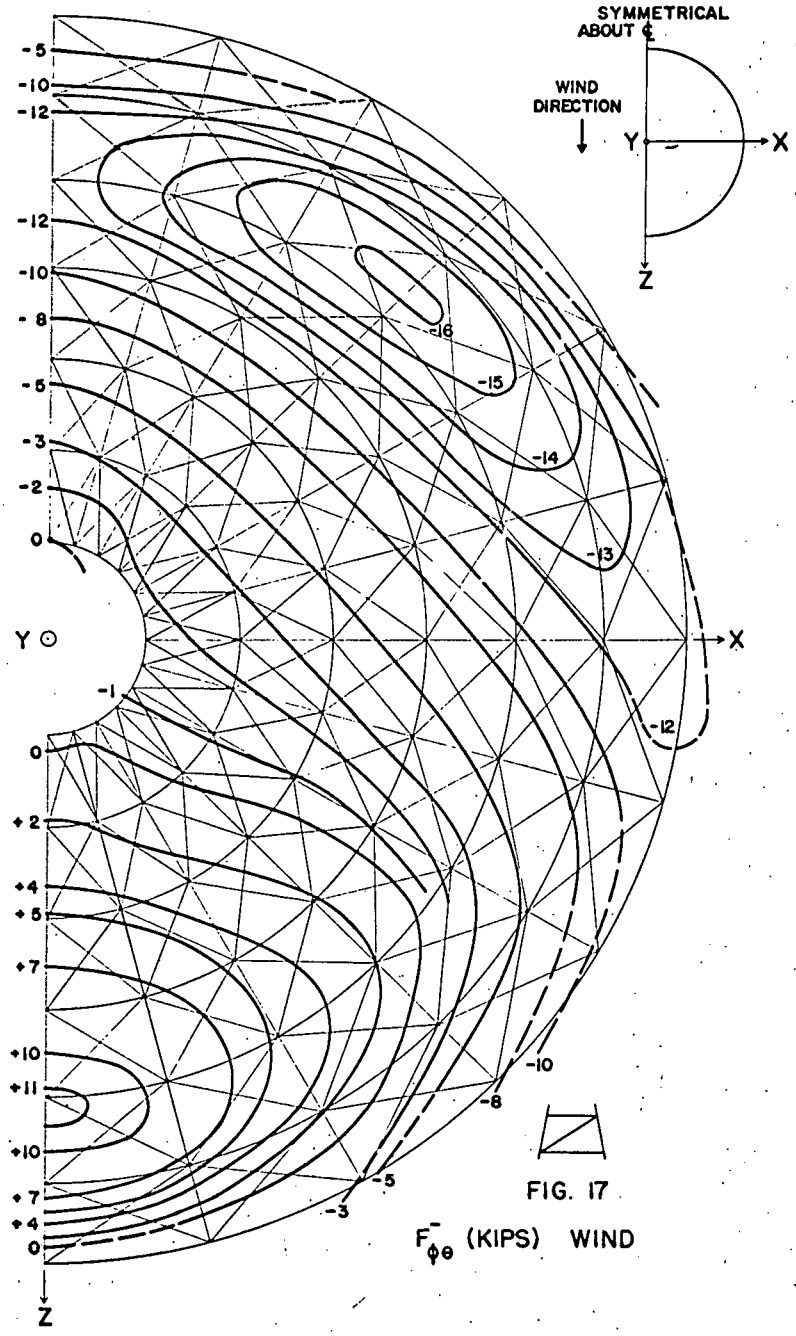

FIG. 17

$F^{-}_{\phi\theta}$ (KIPS) WIND

The wind loading has a significant effect on the internal forces in some cases. Table 3 compares the maximum forces due to wind with those due to full snow.

TABLE 3. MAXIMUM INTERNAL FORCE COMPARISON (WIND)

ϕ degrees		31	26	21	17	12	7
F_ϕ kips	Wind	±11.6	±1.6	±3.5	±4.3	±2.7	±0.4
	U.D.L.	-82.3	-58.0	-36.5	-20.1	-10.5	-6.7
	%	14.1	2.8	9.6	21.4	25.7	6.0
V_ϕ kips	Wind	±1.03	±0.56	±0.34	±0.07	±0.03	±0.04
	U.D.L.	0.91	-0.49	-0.11	0.15	-0.08	-0.39
	%	113	114	309	46.6	37.5	10.3
$F_{\phi\theta}$ kips	Wind	±13.4	±15.9	±13.3	±8.7	±4.6	±2.1
	U.D.L.	-5.18	-16.7	-20.6	-19.5	-15.1	-9.56
	%	259	95.3	64.5	44.6	30.4	22.0
ϕ degrees		28.6	23.9	19.1	14.3	9.5	4.8
M_ϕ ft-kips	Wind	±15.6	±7.1	±2.0	±0.9	±0.5	±0.1
	U.D.L.	13.8	6.40	4.70	6.89	5.75	-0.20
	%	113	111	42.6	13.1	8.7	50.0
F_θ kips	Wind	±9.6	±13.8	±13.4	±11.7	±8.8	--
	U.D.L.	-1.94	-11.6	-18.1	-23.6	-29.1	--
	%	495	119	74.0	49.6	64.7	--

Table 4 shows the eccentricity, e, of the rib axial force and the ratio, η, of the bending stress to the axial stress for the worst stressed rib. Values due to full snow are shown for comparison. It should be noted that under wind action the lower rib segments of the standard dome are primarily bending members.

TABLE 4. ECCENTRICITY OF THE FORCE Fϕ (WIND)

ϕ degrees	Wind e in.	η	Full Snow e in.	η
28.6	16.2	3.2	2.0	0.40
23.9	24.5	4.9	1.3	.26
19.1	5.6	1.1	1.6	.31
14.3	2.5	0.5	4.1	.82
9.5	2.3	.5	6.6	1.32
4.8	3.5	.7	0.4	0.07

2.4 Perimeter Ring Forces

Bending moment and shear forces normal to the plane of the perimeter ring are negligible. Similarly, it was found that shear in the plane of the perimeter ring was generally trivial, most values being less than 0.010 kips and the maximum value being 0.642 kips due to half-snow loading. Table 5 summarizes the forces F_θ and M_θ, for the perimeter ring for half snow (H.S.), wind, and full snow (U.D.L.). Theoretically, the values listed for M_θ under the column heading 'U.D.L.' should be zero. This discrepancy is due to round-off error.

The stress analysis of the perimeter ring of the standard dome may be found in Section 3.2.5.

2.5 Displacements of the Standard Dome

A detailed presentation of the joint displacements of STD is not an objective of this thesis; however, it is important to indicate the magnitude of the displacements. No component of a joint displacement exceeded one inch, consequently no joint translated more than $\sqrt{3}$ inches. In fact, only one joint was found to move more than one inch, and this was due to half snow.

Half-snow loading caused the perimeter ring to have a maximum horizontal displacement of 0.135 in. Comparable values due to wind load and full snow were 0.012 in. and 0.162 in. respectively.

TABLE 5. PERIMETER RING FORCES OF THE STANDARD DOME

θ	F_θ kips			M_θ ft-kips		
degrees	H.S.	Wind	U.D.L.	H.S.	Wind	U.D.L.
0				0.570	-0.827	0.036
	46.7	-39.1	292			
15				0.472	-0.803	-0.024
	48.6	-36.4	292			
30				0.045	-0.725	0.007
	53.2	-31.3	292			
45				-1.25	-0.587	-0.001
	62.6	-24.0	292			
60				-5.53	-0.411	0.007
	81.4	-15.1	292			
75				-16.7	-0.212	-0.024
	120	-5.14	292			
90				0.004	0.0	0.036
	172	5.14	292			
105				16.7	0.212	-0.024
	211	15.1	292			
120				5.52	0.410	0.007
	230	24.0	292			
135				1.25	0.587	-0.001
	239	31.3	292			
150				-0.036	0.725	0.007
	244	36.4	292			
165				-0.494	0.802	-0.024
	245	39.1	292			
180				-0.535	0.827	0.036

The lantern ring had maximum vertical and horizontal displacements of 0.819 in. and 0.255 in. respectively when half-snow loading was applied; maximum values for wind loading were 0.024 in. and 0.116 in.. Vertical and horizontal displacements caused by full snow were 0.602 in. and 0.081 in. respectively.

Total displacements of the rib joints reached maximum values at about $\phi = 17^\circ$, the greatest of which was about one inch caused by half-snow loading. The maximum total displacement caused by wind was about 0.28 in. and that caused by full snow was about 0.85 in..

All of the above displacements are with respect to the geometry of the unloaded dome.

2.6 Stress Analysis of the Web Members and Rib

2.6.1 Criteria

Some results of the stress analysis of the members chosen for the web and rib are presented to show that the sizes were reasonable for a linear analysis of the standard dome. Maximum compressive forces were always greater than or equal to the maximum tensile forces for any particular member.

Values chosen below for allowable stresses are representative of current engineering practice for the design of glued-laminated timber as specified by CSA 086-1959, Code of Recommended Practice for Engineering Design in Timber, including revisions to February, 1961. The Appendix to this thesis summarizes the pertinent parts of this specification.

2.6.2 Live Load Stress Analysis

Diagonal Members

Maximum $F_{\phi\theta}$ = -39.9 kips (compression) half snow $\phi = 26^{o}$

Section 5.0 in. by 15.0 in.

therefore $f_a = \frac{39.9(1000)}{75.0} = 530$ psi

$\frac{\ell}{d} = \frac{13.9(12)}{5.0} = 33$, therefore $F_a = 460$ psi

$\frac{f_a}{F_a} = \frac{530}{460} = 1.15$ satisfactory for short term loading

Web Ring Members

Critical F_θ = -44.3 kips (compression) half snow $\phi = 9^{o}$

Section 5.0 in. by 10.0 in. (assume full support in 5" direction)

therefore $f_a = \frac{44.3(1000)}{50.0} = 885$ psi

$\frac{\ell}{d} = \frac{7.85(12)}{10.0} = 9.4$, therefore $F_a = 2070$ psi

$\frac{f_a}{F_a} = \frac{885}{2070} = 0.43$ satisfactory

Rib Members

Maximum F_ϕ = 82.3 kips (compression) full snow
Corresponding M_ϕ = 13.8 ft-kips at $\phi = 28.6^\circ$

Section 5.0 in. by 30.0 in. (assume full support in 5" direction)

therefore $f_a = \frac{82.3(1000)}{150.0} = 550$ psi

$$f_b = \frac{6(13.8)(12)(1000)}{5.0(30.0)^2} = 220 \text{ psi}$$

$\frac{\ell}{d} = \frac{15(12)}{30.0} = 6$, therefore $F_a = 2070$ psi

$F_b = 2210$ psi

$\frac{f_a}{F_a} + \frac{f_b}{F_b} = \frac{550}{2070} + \frac{220}{2210} = 0.266 + 0.10 = 0.37$ satisfactory

Maximum V_ϕ = 1.26 kips half snow, $\phi = 31^\circ$

$f_v = \frac{1.5(1.26)(1000)}{150.0} = 12.6$ psi satisfactory, since

$F_v = 190$ psi .

It should be noted that even though $\frac{f_b}{f_a} = 4.9$ for wind (Table 4), this condition did not govern design because of the low value of F_ϕ. In fact, the ratio $\frac{f_a}{F_a} + \frac{f_b}{F_b}$ for this segment of the rib was 0.16.

CHAPTER III

EFFECT OF PARAMETER VARIATION

3.1 Introduction

Having obtained an analysis of the preliminary framed dome, the designer may wish to improve the choice of members by studying the effect on the force analysis of variations in some parameters as outlined in Chapter I. Furthermore, he may be concerned only with the maximum forces which any one member may resist. For the standard dome, it is convenient to show in Figs. 18 to 26 how these maximum forces change with the alteration of some parameters. The variation in the tensile values of $F\phi$ has been omitted for half snow because, at any angle ϕ, the maximum tensile value was always less than the maximum compressive value.

3.2 Variation of the Perimeter Ring Size

3.2.1 Properties of the Domes PR1 and PR2

One of the most significant members of a framed dome is the perimeter ring. Its function is to resist the horizontal thrust of the ribs. In this study, each rib was supported by a vertical column with pinned ends, hence the significant parameter was the resistance of this large ring to axial deformation and also to bending in the plane of the ring. These resistances are functions of the cross-sectional area, A, and the moment of inertia, I_y.

Two variations of the standard dome were PR1 and PR2. These domes were identical to the standard dome except that their perimeter rings were modified as shown in Table 6, page 37. The effect of this parameter is displayed by the curves PR1 and PR2 of Figs. 18 to 26.

3.2.2 General Effect on Web and Rib Forces

As would be expected from the theory of shells, the effect of the change in the stiffness of the perimeter ring was greatest near the ring. Greater effect was created by the smaller ring of PR1 than by the larger ring of PR2. The ratios shown in Table 6 indicate that the relative effect found might have been expected since the changes in the perimeter ring properties between PR1 and STD are greater than the changes between STD and PR2.

Near the perimeter ring, rib forces decreased and web forces increased as this ring was stiffened. The changes in some of the force maxima were very great. In particular, the variation in the forces $V\phi$ and $M\phi$ for half-snow loading should be noted (Figs. 19 and 20). Near the lantern ring the relative changes were small.

3.2.3 Change in Stresses

Fig. 22 shows that stiffening the perimeter ring reduced the maximum $F_{\phi\theta}$ in the critical panel of STD ($\phi = 26^{\circ}$) from -39.9 kips to -37.8 kips; thus the actual stress was reduced and the ratio of the actual to the allowable stress was improved from 1.16 to 1.10. At $\phi = 31^{\circ}$, however, the actual stress rises causing this ratio to become 1.12. No other change was significant.

Maximum values of the web ring force, F_{θ}, changed greatly in only one case. At $\phi = 28.6^{\circ}$, the maximum tensile force caused by half-snow loading increased from 4.59 kips for STD to 7.42 kips for PR1 (Fig. 21).

Shear forces, V_{ϕ}, and consequently bending moment, M_{ϕ}, were very sensitive to changes in the ring girder stiffness (see Figs. 19 and 20, 24 and 25). To a lesser degree F_{ϕ} changes also (Figs. 18, 23). However, the worst stresses in the ribs of PR1 and PR2 were still caused by full-snow loading. Table 7 shows the ratios of the three rib force maximum values compared to those of the standard dome for the worst stressed rib segments. The combined stress ratio for these segments of PR1 was still satisfactory (0.75) provided that the same criteria were assumed (section 2.6.4).

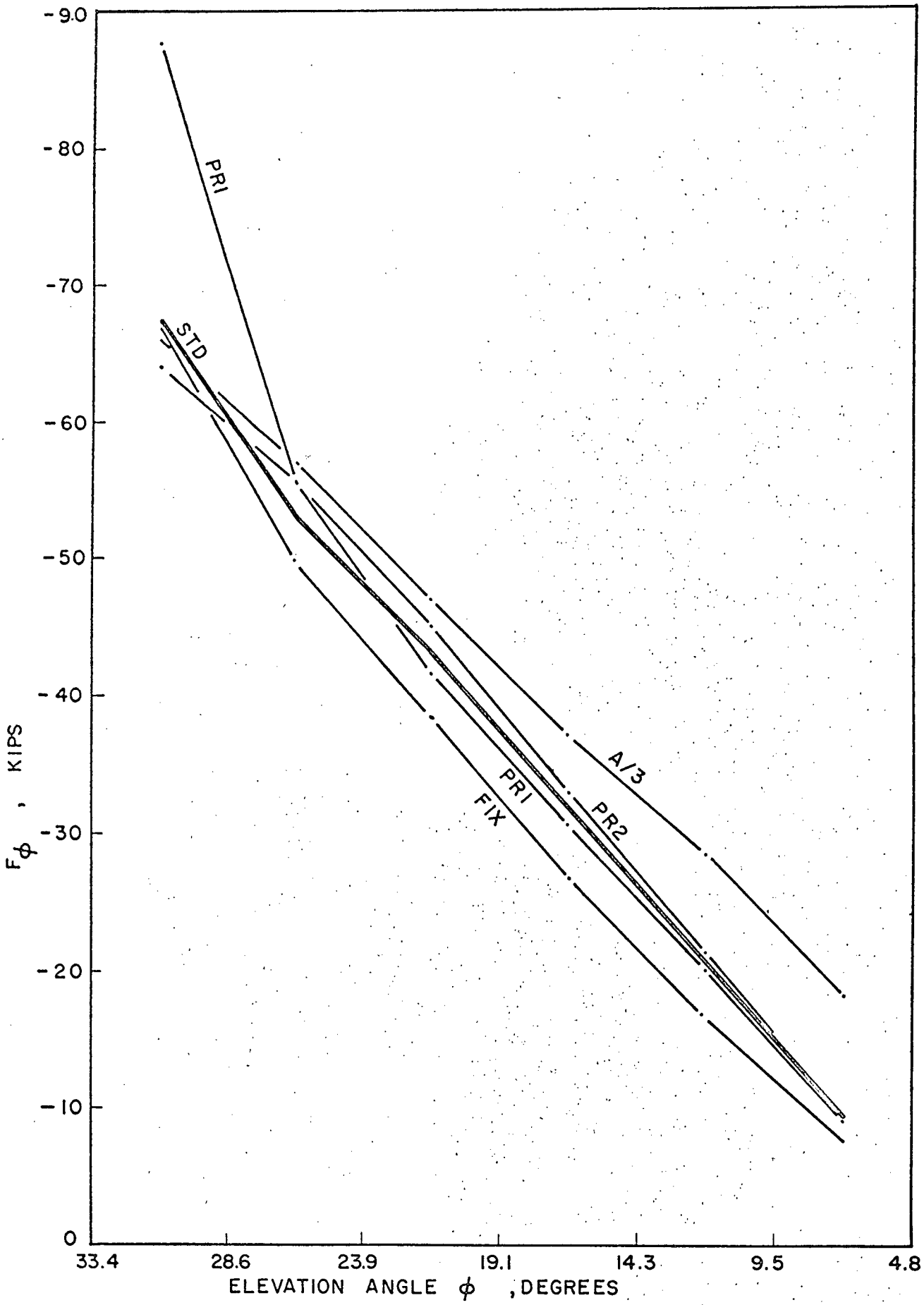

FIG. 18 MAXIMUM COMPRESSIVE F_ϕ HALF SNOW

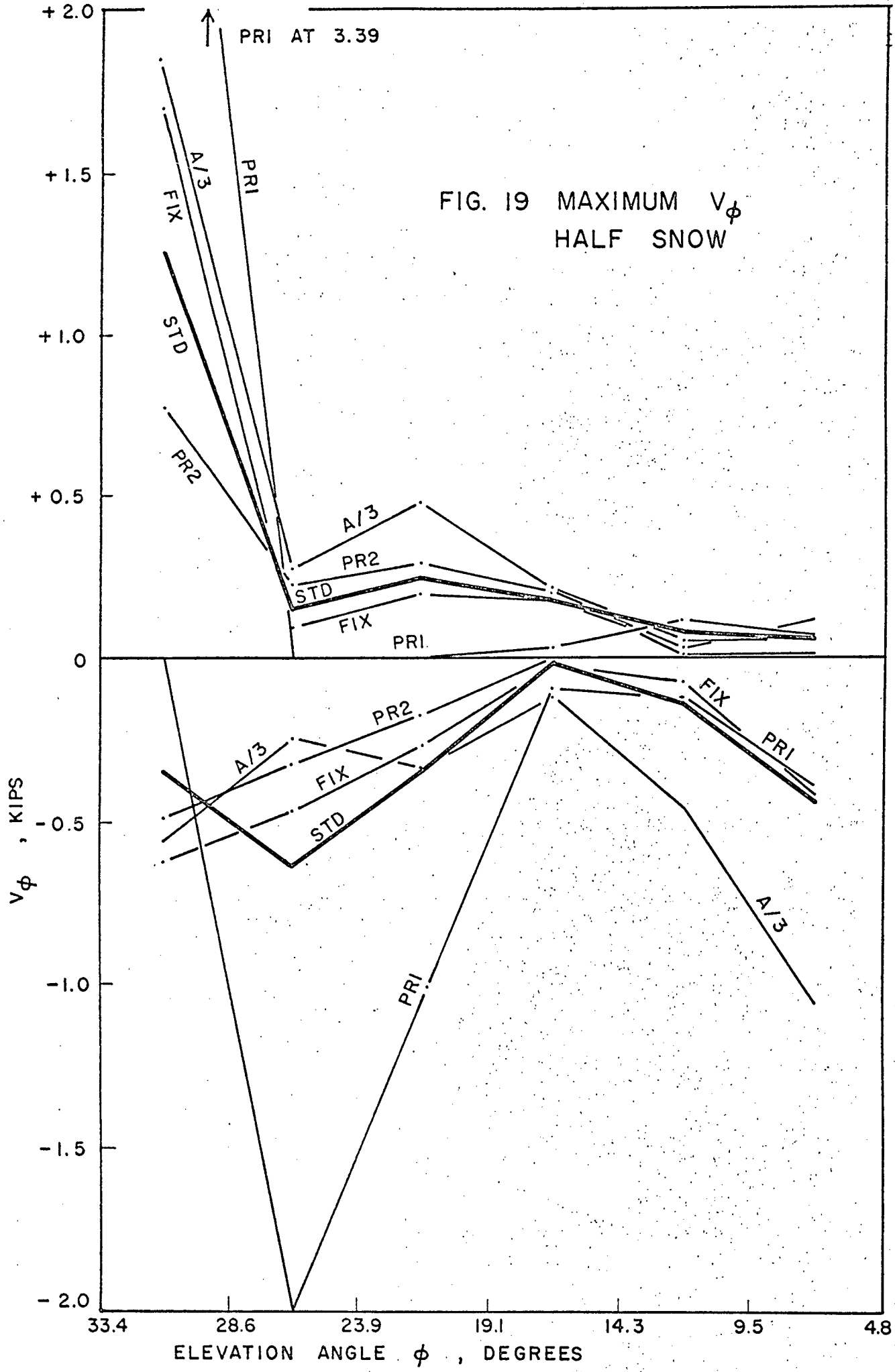

FIG. 19 MAXIMUM V_ϕ
HALF SNOW

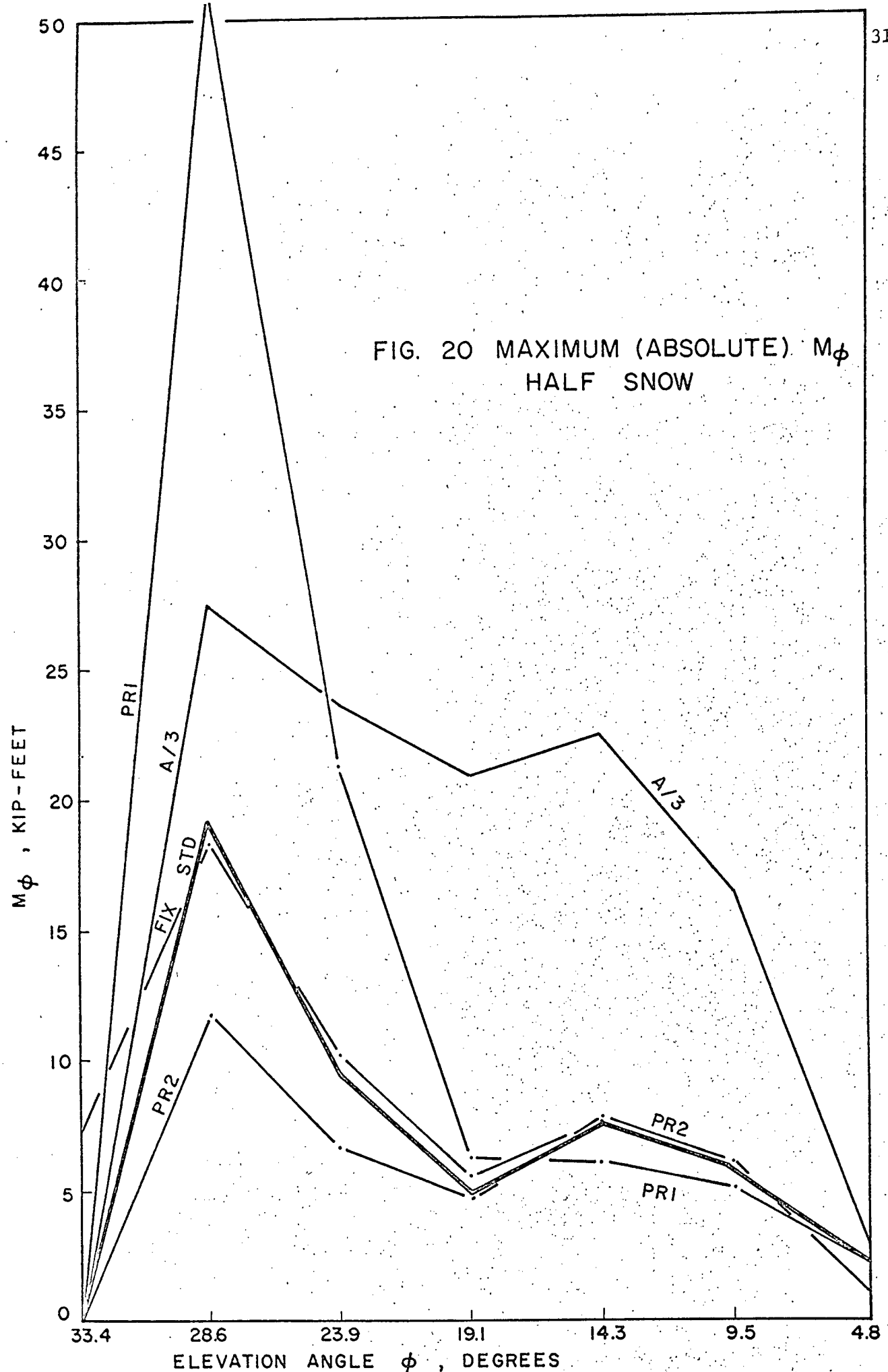

FIG. 20 MAXIMUM (ABSOLUTE) M_ϕ
HALF SNOW

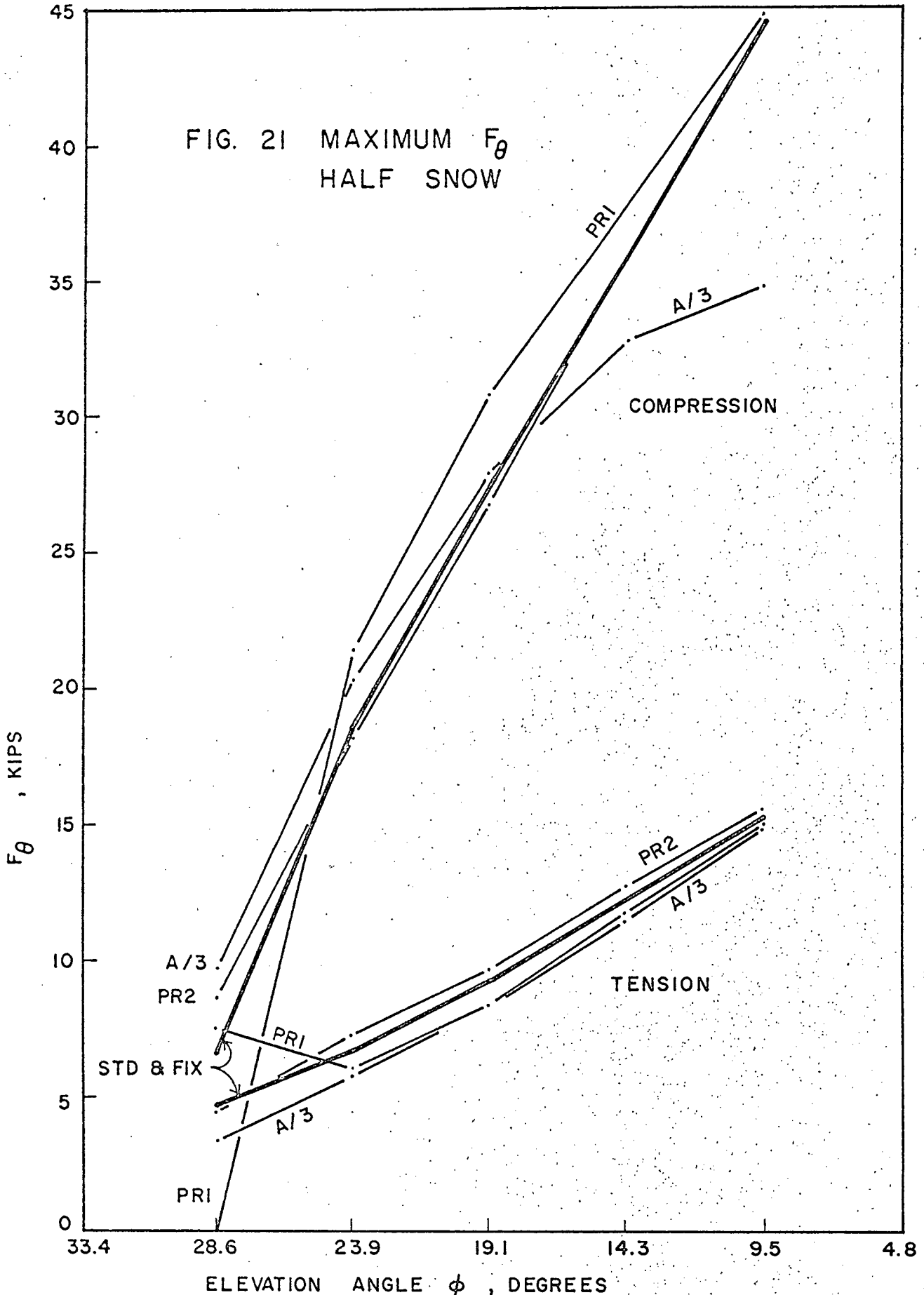
FIG. 21 MAXIMUM F_θ
HALF SNOW
PRI
A/3
COMPRESSION
PR2
A/3
TENSION
A/3
PR2
PRI
STD & FIX
A/3
PRI
F_θ , KIPS
0
5
10
15
20
25
30
35
40
45
33.4
28.6
23.9
19.1
14.3
9.5
4.8
ELEVATION ANGLE ϕ , DEGREES

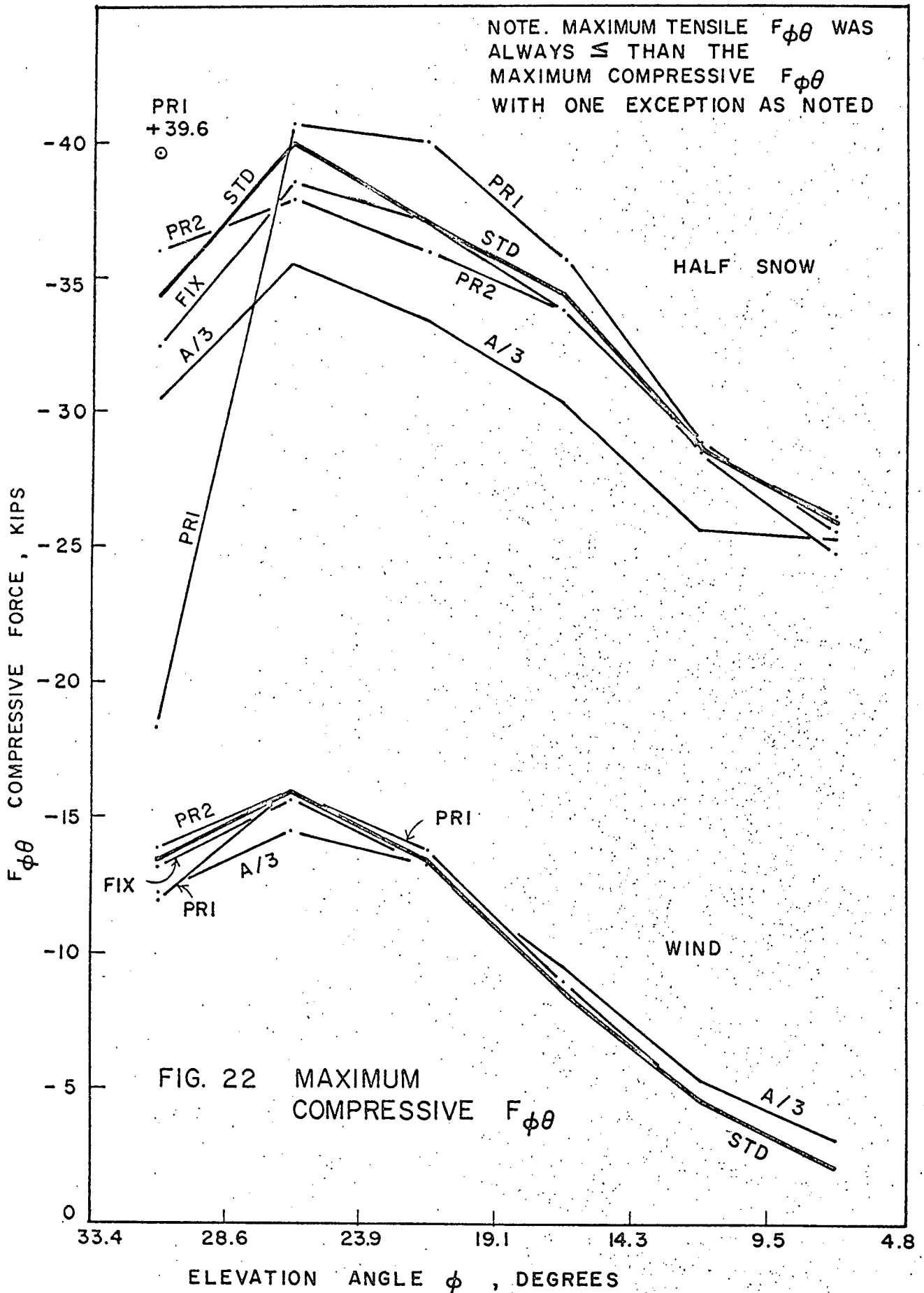

FIG. 22 MAXIMUM COMPRESSIVE $F_{\phi\theta}$

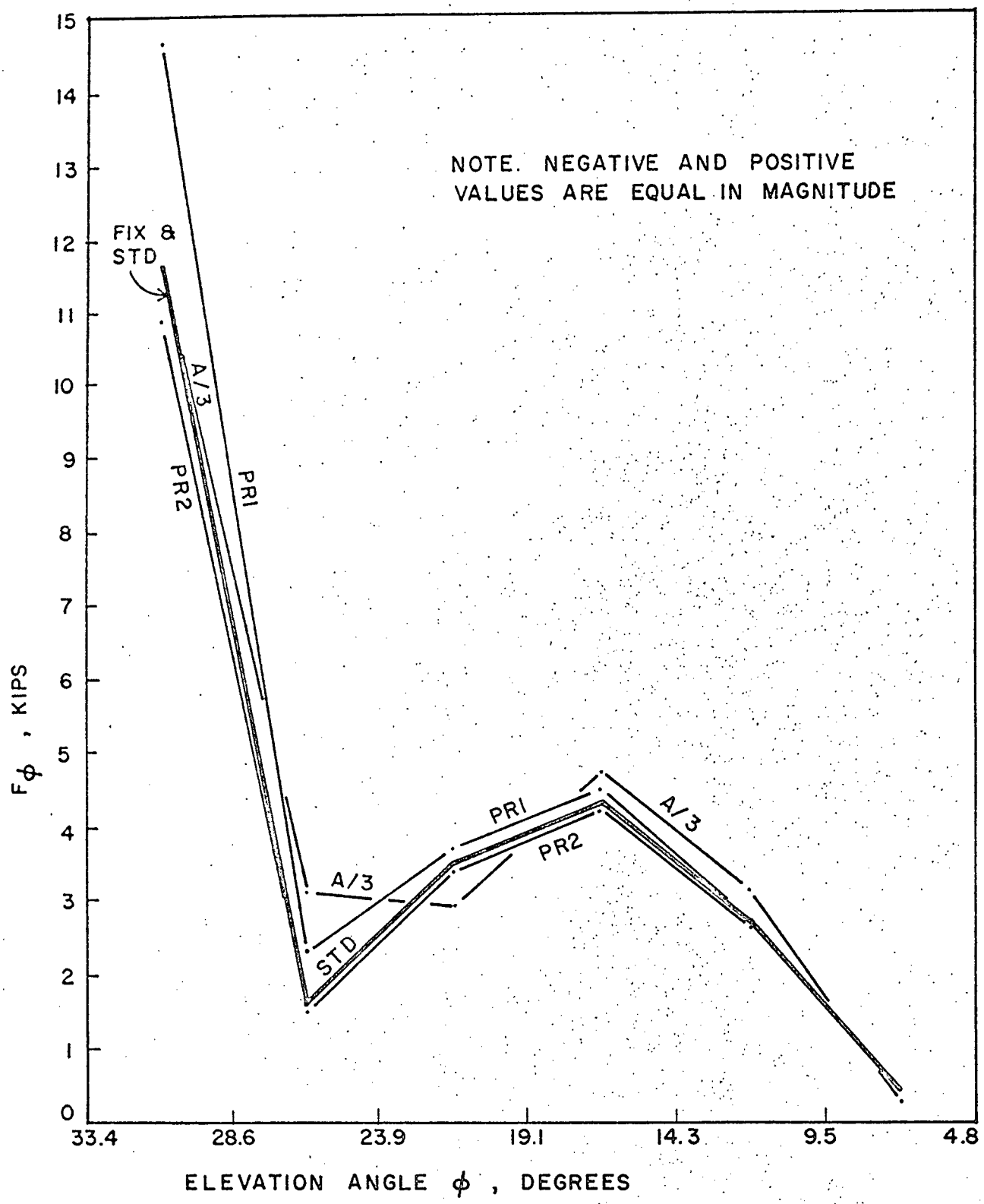

FIG. 23 MAXIMUM F_ϕ WIND

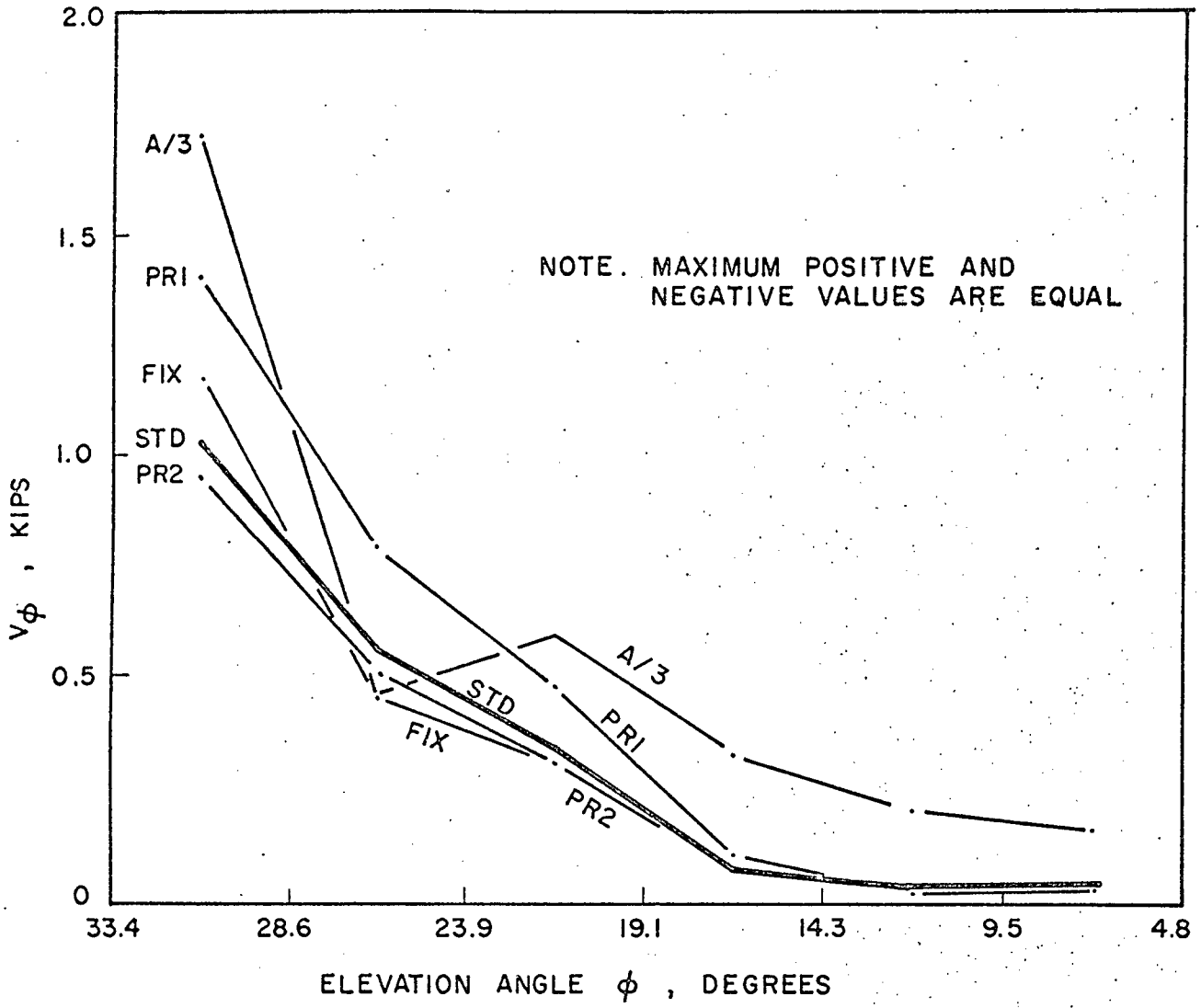

FIG. 24 MAXIMUM V_ϕ WIND

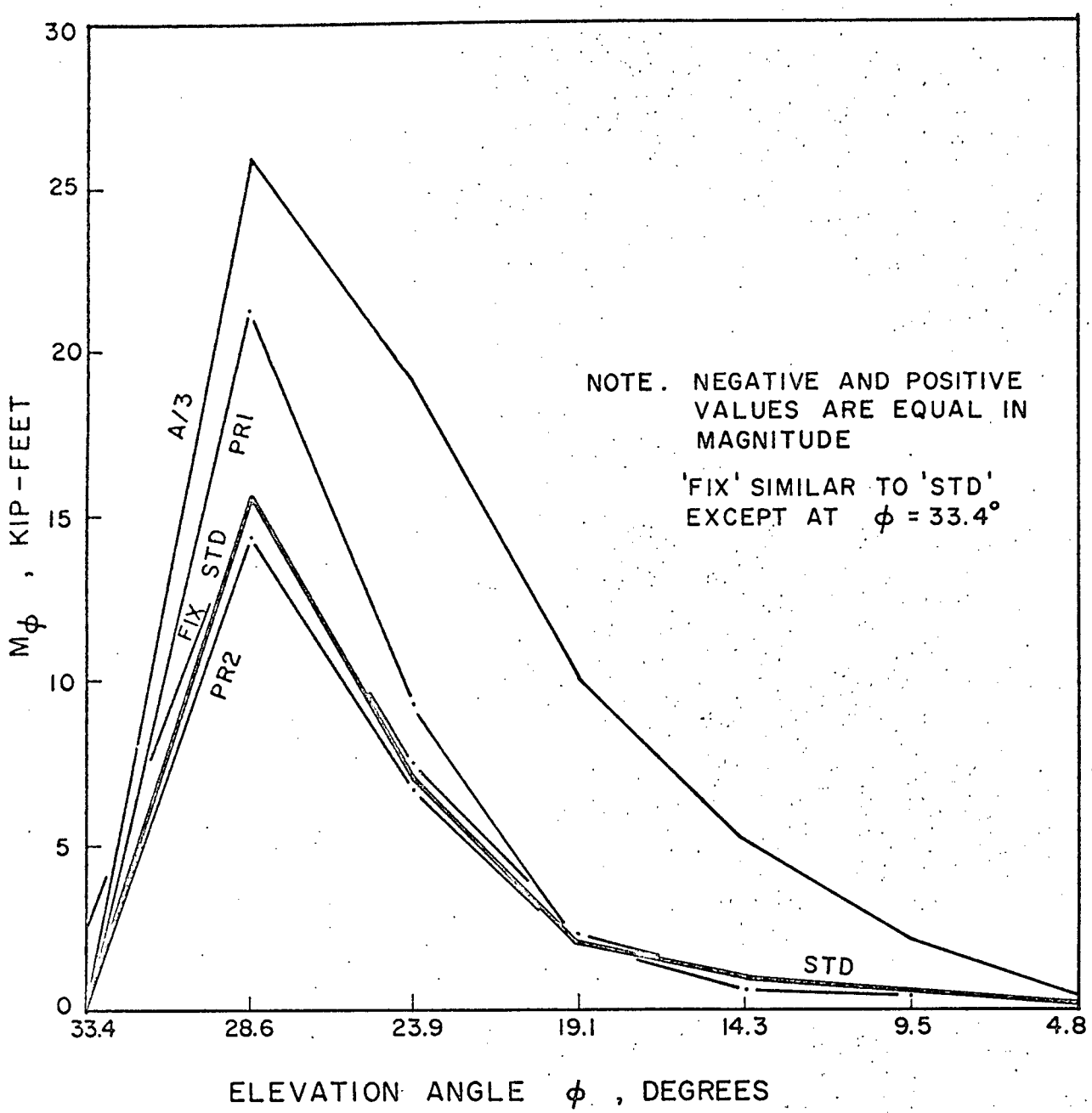

FIG. 25 MAXIMUM M_ϕ WIND

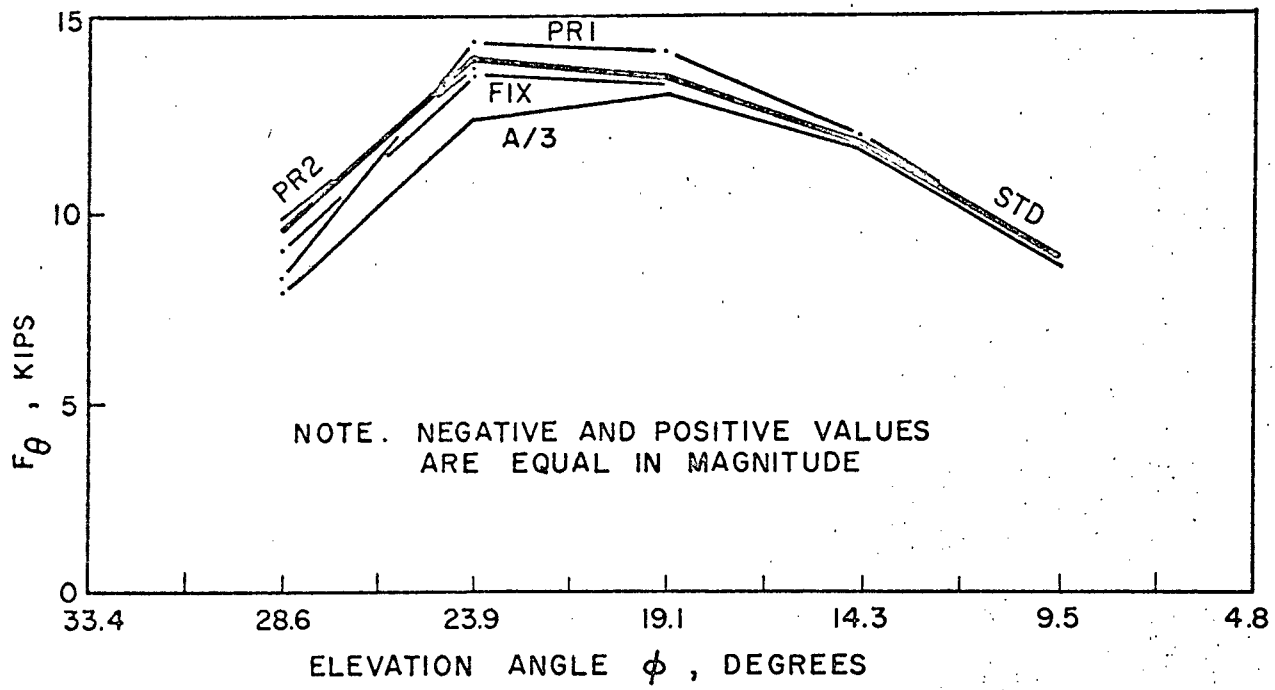

FIG. 26 MAXIMUM F_θ WIND

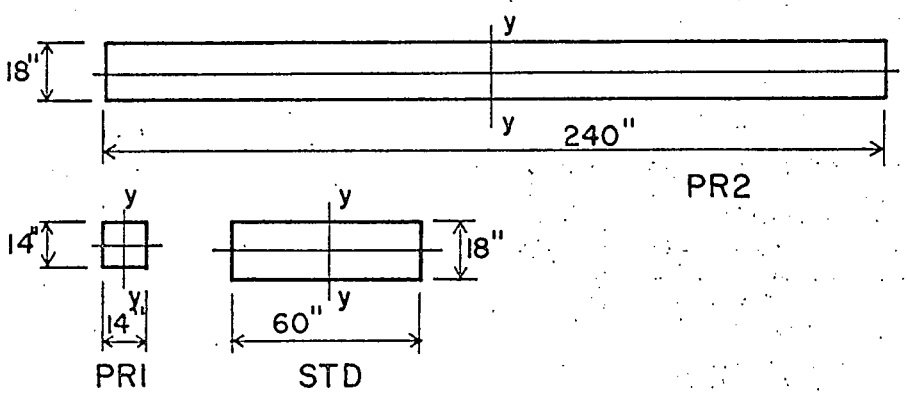

CODE	A	I y
PRI	200 in^2	3,330 in^4
STD	1080	324,000
PR2	4320	20,700,000
Ratio of PRI and PR2 to STD		
PRI	0.185	0.010
STD	1.0	1.0
PR2	4.0	64.0

TABLE 6. SIGNIFICANT PROPERTIES OF THE PERIMETER RINGS

TABLE 7. RATIOS OF RIB FORCES FOR FULL-SNOW LOADING

Dome	ϕ	F_ϕ	M_ϕ	V_ϕ
PR1	28.6°	1.28	4.09	4.09
STD		1.0 (-82.3 k)	1.0 (13.8 ft-k)	1.0 (0.91 k)
PR2		0.88	0.31	0.31
PR1	23.9°	1.10	3.63	4.45
STD		1.0 (-58.0 k)	1.0 (6.40 ft-k)	1.0 (-0.49 k)
PR2		0.98	0.41	0.22

3.2.4 Change in Displacements

Tables 8 and 9 show the relative maximum displacements of domes PR1 and PR2 compared to those of the standard dome, STD, which are described in section 2.5 above and recorded again for convenience. Symbols ΔV and ΔH are, respectively, maximum vertical and maximum horizontal displacement ratios. The notation ΔMAX is the ratio of the maximum total translations found in the web and rib portion of the dome.

3.2.5 Changes in the Perimeter Ring Forces

Variation of the perimeter ring properties caused changes in the forces within itself. A comparison of the forces F_θ and M_θ of the perimeter rings of domes PR1 and PR2 with those of STD (Table 5, section 2.4), revealed that, for F_θ and wind or full snow, PR1 values were 20% lower than STD values and PR2 values were 4-1/2% higher than STD values. For F_θ and half snow, PR1 values ranged from 16 to 25% lower than STD values and PR2 values were 7% higher than STD values.

The M_θ values of the perimeter ring of PR1 were very small, never exceeding 0.284 ft-kips. This value is comparable to the 16.7 ft-kips of STD at $\theta = 75^\circ$ under half snow (Table 5). The comparable value for PR2 was the maximum value of 214 ft-kips. It is obvious that increasing the stiffness of the perimeter ring increases its internal forces significantly, particularly the moment acting in the plane of the ring; however, the stresses which arise are small as shown in Table 10.

TABLE 8. RATIOS OF MAXIMUM DISPLACEMENTS OF 'PR1' AND 'PR2' PERIMETER AND LANTERN RINGS COMPARED TO 'STD'

Dome	Half Snow		Wind		Full Snow	
	ΔV	ΔH	ΔV	ΔH	ΔV	ΔH
Perimeter Ring						
PR1	1.77	2.24	1.50	6.60	1.71	4.32
STD	1 (.022")	1 (.135")	1 (.006")	1 (.012")	1 (.026")	1 (.162")
PR2	0.86	0.63	1.0	1.25	0.85	0.26
Lantern Ring						
PR1	1.58	0.61	1.58	0.67	2.50	0.98
STD	1 (.819")	1 (.255")	1 (.024")	1 (.116")	1 (.602")	1 (.081")
PR2	0.87	1.10	0.83	1.07	0.67	1.00

TABLE 9. RATIOS OF MAXIMUM DISPLACEMENTS OF 'PR1' AND 'PR2' COMPARED TO 'STD', AT ABOUT $\phi = 17^{o}$

Dome	Half Snow	Wind	Full Snow
	ΔMAX	ΔMAX	ΔMAX
PR1	1.68	1.55	2.20
STD	1 (1.0")	1 (0.28")	1 (0.85")
PR2	0.87	0.97	0.69

TABLE 10. PERIMETER RING STRESS COMPARISON, PSI

Dome	Half Snow		Wind		Full Snow	
	f_a	f_b	f_a	f_b	f_a	f_b
PR1	992	7	156	1	1170	0
STD	227	19	36	1	271	0
PR2	60	15	9	1	71	0

Note: Values shown are maximum values and do not necessarily exist in the same member.

3.3 Web Member Area Reduction

3.3.1 Properties of the Dome A/3

The web members of a framed dome are required to provide a direct resistance to shear forces arising from loadings which are not axi-symmetric. The diagonals and intermediate rings of the standard dome were pin-connected to the ribs. To assess the effect of these web members on the internal force distribution of STD, a new dome, A/3, was analyzed. It was identical to STD except that the areas of the diagonals and intermediate rings were two-thirds smaller; that is, 25.0 $in.^2$ and 16.67 $in.^2$ respectively.

3.3.2 General Effect on Web and Rib Forces

Comparison of the maximum forces in dome A/3 with those of STD indicates that the greatest effect occurred in the higher elevations. Rib forces were more affected than web forces, particularly the bending moment, M_ϕ. Generally, the reduction in web member areas increased the rib force maximums and decreased the web force maximums. Exceptions to this rule, at certain values of ϕ, were increases in F_θ and $F_{\phi\theta}$.

3.3.3 Change in Stresses

The maximum $F_{\phi\theta}$ forces created by half-snow loading decreased at all angles of ϕ, however, this trend was not always true for wind loading (Fig. 22). It was also evident that maximum actual stresses in the diagonals, caused by half snow, were now above allowable stresses if the same buckling criteria of STD were assumed. The actual stresses in the diagonals of dome A/3 ranged from 1000 psi to 1415 psi and the highest ratio of actual to allowable stress was 3.08.

The maximum compressive F_θ forces created by half snow increased at lower elevations but decreased at the higher elevations, whereas F_θ forces decreased at all angles of ϕ for wind loading (Figs. 21, 26). The maximum

compressive stresses, caused by half snow, ranged from 580 psi to 2070 psi and the ratio of actual to allowable stresses reached a maximum of 1.30.

Rib forces were increased by the web member area reduction, particularly in the higher elevations, however, since the rib was of constant cross-section these greater forces were of little consequence. The highest stresses were created by half-snow loading ($F_\phi/A + M_\phi/S = 880$ psi), but the highest combined stress ratio was created by full snow (0.40). Shear stresses in the rib did not exceed 20 psi.

3.3.4 Change in Displacements

Displacements of A/3 were generally greater than the comparable values of STD which will appear in parentheses. Half-snow loading caused the perimeter ring to have a maximum horizontal displacement of 0.148 in. (0.135); maximum horizontal wind loading displacement was 0.015 in. (0.012). Full snow created a maximum horizontal displacement of 0.163 in. (0.162).

The lantern ring had maximum vertical and horizontal displacements of 1.309 in. (0.819) and 0.813 in. (0.255) respectively, owing to half snow; maximum values for wind loading were 0.093 in. (0.024) vertically and 0.335 in. (0.116) horizontally. Vertical and horizontal displacements caused by full snow were 0.231 in. (0.602) and 0.101 in. (0.081) respectively.

Total displacements of the rib joints reached maximum values at about $\phi = 17^\circ$, the greatest of which was 2.2 in. caused by half snow. The maximum total displacements caused by wind loading and full snow were about 1.0 in. and 1.4 in. respectively.

3.4 Change in Member End Condition

3.4.1 The Pinned-End Condition

The end conditions characteristic of the standard dome are useful for fabrication and erection purposes. Many analyses of such structures have been

made based on the assumption that all members were pin-connected. To assess the differences which must exist between the standard dome and a similar dome which is completely pin-connected, a computer analysis was attempted which needed only three translatory degrees of freedom per joint. A solution was not obtained. Negative terms appeared on the diagonal of the lower triangular matrix L during the decomposition of the structure stiffness matrix K to LL^T. Since K is symmetric and positive-definite, negative terms must be due to round-off error. The matrix order was then reduced by analyzing one quarter of the dome. While the diagonal terms of L remained positive, the displacements of the joints of the lantern ring were in the order of 210 ft when the loading was uniformly distributed. The pin-connected dome was abandoned at this point. Double precision, instead of the eight significant figures used, or an iteration technique, might have provided a reasonable solution.

3.4.2 The Fixed-End Condition

Today, with the advent of shop and field welding, it is possible to provide rigid connections between member ends. To study the effects of such connections, all the joints of the standard dome were fixed to form a new dome, FIX. The web members were aligned such that their y-y axes lay in planes which passed through the spherical centre of the dome.

Comparison of FIX with STD showed that for the half-snow loading, all maximum forces were decreased with the exception of V_ϕ and M_ϕ which increased at certain values of ϕ. For wind loading, only the maximum value of V_ϕ increased significantly (Fig. 24) and this increase occurred next to the perimeter ring. The effect of this parameter was small except on the maximum values of F_ϕ and V_ϕ created by half snow (Figs. 18 and 19).

Figs. 21, 22, and 26 show the very small change in $F_{\phi\theta}$ and F_θ forces caused by fixing all joints. It follows that the actual stresses are similar to those of STD (section 2.6). Furthermore, Figs. 18 to 20, 23 to 25, show

little difference between FIX and STD for the rib forces. Also, the rib forces in the dome FIX caused by full snow were similar to those of STD, the critical forces differing by less than 4%.

Fixing the ends of the web members introduces into these members the bending forces of the 'Fixed Member' of Fig. 3. A consideration of these bending forces should be made for the proper design of the web members but since only the axial force is being studied, these bending forces will be left to a later study.

Displacements of the dome FIX were generally smaller than the comparable values of STD which will appear in parentheses. The displacements of the perimeter ring were identical to those of STD.

Half-snow loading caused the lantern ring to have a maximum vertical displacement of 0.779 in. (0.819) and a maximum horizontal displacement of 0.248 in. (0.255); wind loading displacements were 0.031 in. (0.024) vertically and 0.116 in. (0.116) horizontally. Full snow created displacements of 0.611 in. (0.602) vertically and 0.081 in. (0.081) horizontally.

Total displacements of the rib joints reached maximum values at about $\phi = 17^{\circ}$, the greatest of which was 0.94 in. caused by half snow. The maximum total displacements caused by wind and full snow were about 0.36 in. and 0.81 in. respectively.

3.5 A Local Geometry Change

During the fabrication of structural members, manufacturing tolerances can be exceeded. If, for example, two ring members meeting at the same joint were each shorter than their proper length, then a local depression, or dimple, will occur in the spherical surface defined by the joints. To assess the effect of such a depression, radial changes only were made in the geometry of three joints of one rib of the standard dome as shown in Fig. 27. It is assumed that the other members adjacent to the joints were cut in such a manner

that the resulting dome, GEO, was in a stress-free state after erection. As shown in Fig. 27, the three geometry changes were at $\theta = 180^{\circ}$, the centre-line of the dome and the loadings.

A comparison of the internal forces of domes STD and GEO was made, member by member, which revealed that significant force changes occurred locally in the region of the dimple. Provided that θ was less than 150°, any changes rarely exceeded 5% and never exceeded 20%. The greatest increases in $F_{\phi\theta}$ took place next to the lantern ring; some $F_{\phi\theta}$ values due to wind, were 2.3 times greater in GEO than comparable values in STD. For half snow, the ratio was 1.4 and for full snow 1.2. Ring forces, F_{θ}, changed little, the greatest increase being 7% at $\phi = 28.6^{\circ}$ for full-snow loading.

Rib forces changed significantly because of the dimple. The V_{ϕ} value near the centre of the dimple was 8.63 times greater than that of STD. A corresponding change occurred in M_{ϕ}, the GEO value being 3.82 times greater than that of STD. These increases were for full-snow loading but the half-snow ratios were almost as great. Increases for wind loading were smaller again but still significant. Half-snow loading caused the F_{ϕ} forces of GEO to increase to values about five times greater than those of STD; ratios for wind and full snow were 3.50 and 1.79 respectively.

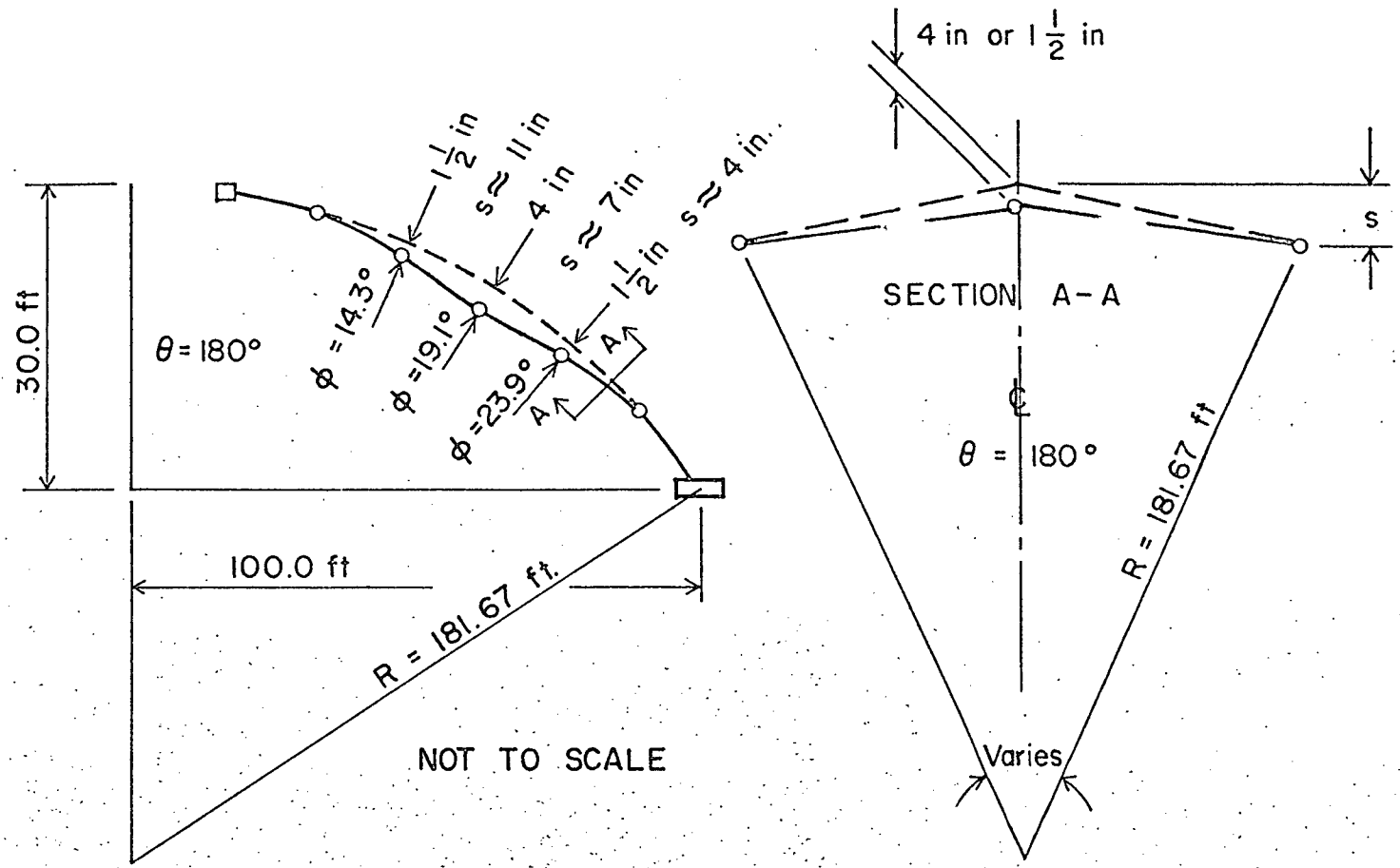

FIG. 27 SPECIAL GEOMETRY OF THE DOME 'GEO'

CHAPTER IV

APPROXIMATING THE MAXIMUM DIAGONAL FORCE

4.1 Past Work

The theory for the analysis of domes subjected to axi-symmetric loadings is well developed by comparison with that developed for unsymmetric loadings. It is known that the diagonal force, $F_{\phi\theta}$, reaches maximum value with unsymmetric loadings, but little information is available to estimate this force and the necessary structural member. The designer without a computer service must determine a diagonal size: the designer with a computer service should determine a reasonable member for the first analysis.

One worker on this problem was W. Schwedler[1] who presented in 1866 an analysis for a framed dome similar in layout to the standard dome. He assumed all loads to be concentrated at the joints and secondary forces due to deflection to be negligible. Furthermore, he considered that only the tension diagonals were effective when a dome is subjected to unsymmetrical loading.

Schwedler suggested that if the dome was loaded on one side of a meridional plane passing through the centre of a panel, then the maximum diagonal forces would be produced in this panel. His approximation was published in a form equivalent to:

$$(F_{\phi\theta})_n < \frac{\sum_{i=1}^{n} L_i}{\sin \alpha_n \cos \beta_n}$$

where n = joint number counting from the lantern ring toward the perimeter ring,

L_i = vertical live load at the joints,

α_n = angle between the rib segment and the horizontal,

β_n = angle between the rib segment and the diagonal.

In presenting this approximation, Schwedler argues that on the loaded side of the dome the rib force is:

$$(F_\phi)_n = \left(\sum_{i=1}^{n} L_i\right) / \sin \alpha_n$$

while on the unloaded side, the rib force is zero. He then assumes that

$$(F_{\phi\theta})_n \cos \beta_n < (F_\phi)_n .$$

In other words, the diagonal force need not be larger than that required to provide the difference in the two rib forces. Schwedler assumes that only the tension diagonal acts and so it transfers all the shear.

Later writers, Benjamin[2] and 'Hütte'[3], modified this formula to this form:

$$(F_{\phi\theta})_n = \frac{\sum_{i=1}^{n} L_i}{2 \sin \alpha_n \cos \beta_n}$$

and still considered it to be conservative.

It is the objective of this chapter to present other approaches for the approximation of the maximum diagonal force, $F_{\phi\theta}$, caused by half snow or wind.

4.2 Half-Snow Loading

A freebody of the framed dome will appear as presented in Fig. 28 if only the internal forces F_ϕ and $F_{\phi\theta}$ are considered. The horizontal tangential component of $F^+_{\phi\theta}$ and $F^-_{\phi\theta}$ divided by the panel width b gives a shear flow V. Note that the meridional component of this sum, and F_ϕ, pass through O and consequently have resultants passing through O.

Inspection of the exact distribution of V indicates that the following parabolic distribution could predict the shear flow:

$$V = V_o \left(\frac{\theta}{\theta_o}\right)^2, \qquad 0 \leqslant \theta \leqslant \theta_o,$$

and

$$V = V_o \left(\frac{\pi-\theta}{\pi-\theta_o}\right)^2, \qquad (\pi-\theta_o) \leqslant \theta \leqslant \pi,$$

where θ_o is the horizontal angle to V_o, the maximum shear flow. The same distribution of V is assumed to exist on the other side of the dome's axis of symmetry. If the first quadrant of θ is considered and θ_o is taken as $\pi/2$

$$V = 4\, V_o \left(\frac{\theta}{\pi}\right)^2, \qquad 0 \leqslant \theta \leqslant \pi/2 \ .$$

The summation for the resultant of V is

$$H = 4\int_o^{\pi/2} V \sin\theta \; r \, d\theta = \frac{16 r V_o}{\pi^2} \int_o^{\pi/2} \theta^2 \sin\theta \, d\theta$$

$$= r V_o 16\,(\pi-2)/\pi^2 = 1.85 r V_o \ .$$

ΣM about point O of Fig. 29 produces

$$H = \frac{Pe}{d}$$

so that

$$V_o = \frac{Pe}{1.85\ rd} \ .$$

This expression for V_o is statically correct if the secondary forces, V_ϕ and M_ϕ, are neglected and depends on a second degree parabola approximation for V.

As a numerical example, for $\phi = 31^\circ$ and the half-snow loading of Fig. 2, there are:

P = 550 kips	e = 0.424 r = 39.7 ft
r = 93.6 ft	d = 56.2 ft

from which $V_o = 2.24$ klf and $V = 2.24 \left(\frac{2\theta}{\pi}\right)^2$ klf .

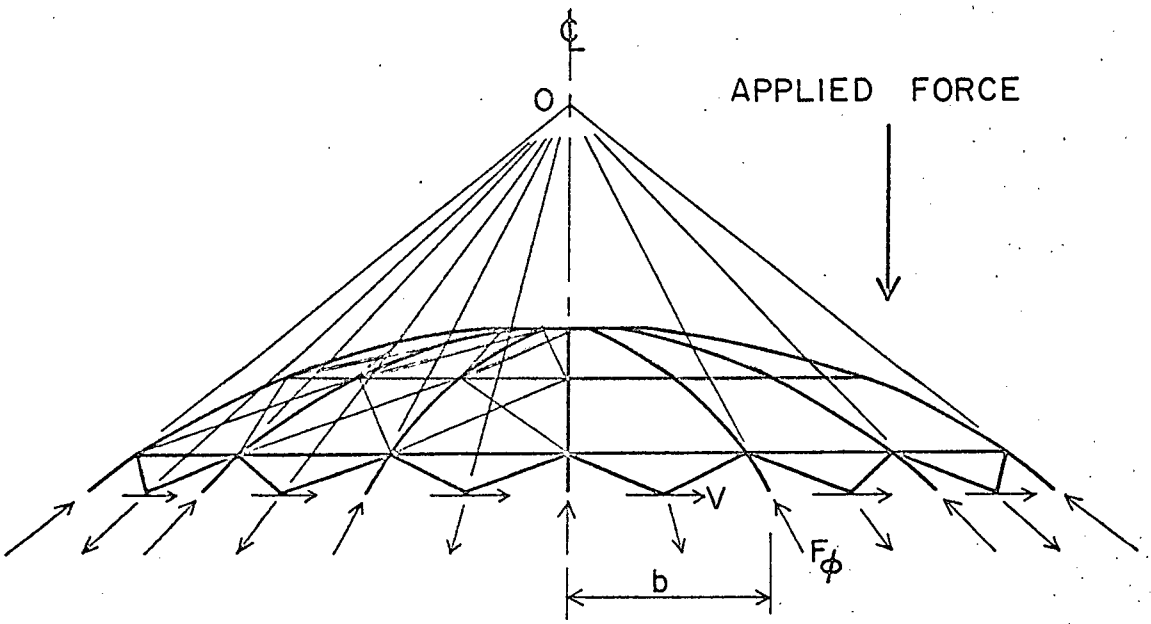

FIG. 28 FREEBODY FOR UNSYMMETRIC LOADING

V_ϕ AND M_ϕ ARE NEGLECTED

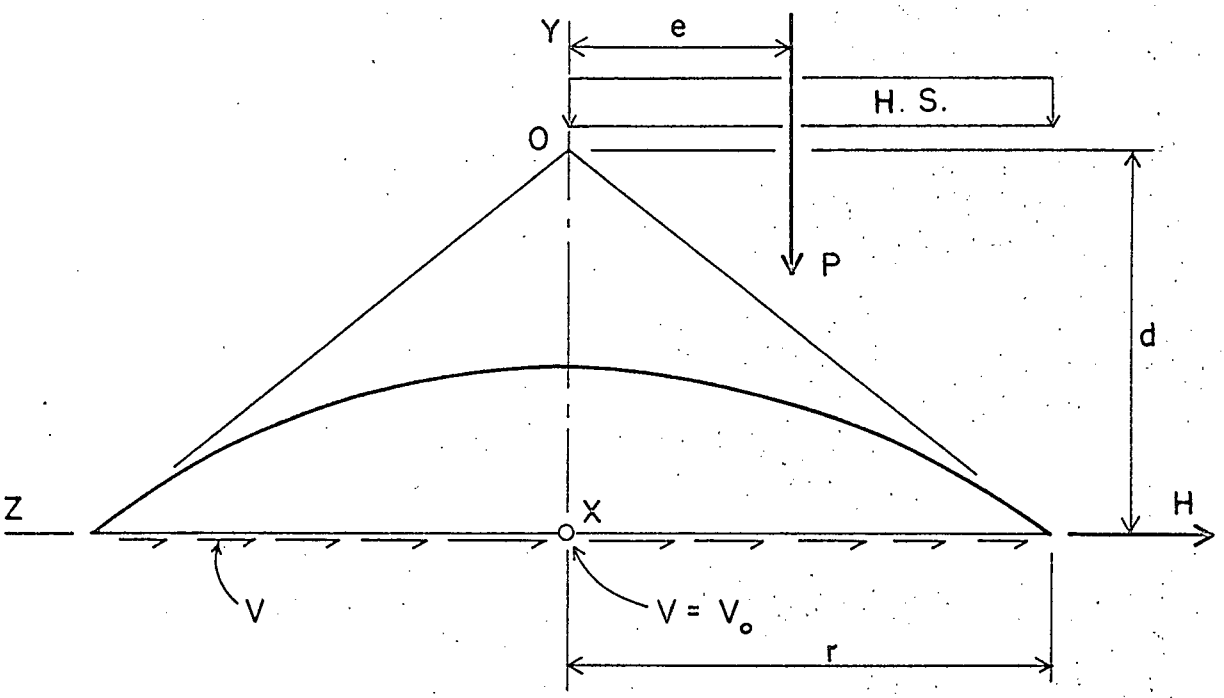

FIG. 29 FREEBODY FOR HALF SNOW

Comparison of this assumed distribution with the exact analysis for domes STD and PR1 is shown in Fig. 30. The calculation for the exact distribution of V is given in Table 11 according to the formula of Fig. 31. The assumed distribution underestimates the actual worst V by 11%. Fig. 30 shows, too, that the influence of the perimeter ring size is not great.

The discontinuity of load at $\theta = 90^{\circ}$ is responsible for the relatively large V_o found in the analysis. In actual practice, it is reasonable to assume that the snow pressure tapers from zero intensity to full intensity over a finite length. This taper produces smaller stresses in a shell.

As a preliminary study, the half-snow loading of Fig. 2 was modified to a zero intensity from θ equals 0° to 60°, a linear increase in intensity to 40 psf from θ equals 60° to 120°, and a uniform intensity of 40 psf from θ equals 120° to 180°.

Inspection of the exact curve of V for tapered snow indicates that the following distribution could predict this shear flow:

$$V = V_o \sin^2 \theta, \qquad 0 \leqslant \theta \leqslant \pi$$

The same distribution of V is assumed to exist on the other side of the dome's axis of symmetry. The summation for the resultant of V is then

$$H = 4 \int_0^{\pi/2} V \sin \theta \, r d\theta = 4rV_o \int_0^{\pi/2} \sin^3\theta \, d\theta = \frac{8rV_o}{3} .$$

ΣM about point O of Fig. 29 produces

$$H = \frac{Pe}{d}$$

so that

$$V_o = \frac{3Pe}{8rd} .$$

This expression for V_o is statically correct if the secondary forces, V_ϕ and M_ϕ, are neglected and is dependent on the approximation for V.

θ degrees	7.5	22.5	37.5	52.5	67.5	82.5	97.5	112.5	127.5	142.5	157.5	172.5
Diagonals defined by $\phi = 31^{o}$												
$F_{\phi\theta}^{-}$ kips	0.67	-1.10	-3.35	-6.89	-13.8	-30.5	-34.3	-21.6	-15.1	-11.6	-9.28	-7.50
$F_{\phi\theta}^{+}$ kips	2.32	4.10	6.37	9.87	16.5	29.1	25.3	8.64	1.71	-1.83	-4.08	-5.85
Diff kips	1.65	5.20	9.72	16.8	30.3	59.6	59.6	30.3	16.8	9.72	5.20	1.65
$\cos\lambda/b$	0.035	→										
V klf	0.058	0.182	0.340	0.587	1.06	2.08	2.08	1.06	0.587	0.340	0.182	0.058
Diagonals defined by $\phi = 26^{o}$												
$F_{\phi\theta}^{-}$ kips	1.65	-0.58	-3.45	-7.81	-15.4	-31.2	-39.9	-34.3	-28.7	-25.0	-22.4	-20.3
$F_{\phi\theta}^{+}$ kips	3.66	5.77	8.35	12.0	17.6	23.2	14.5	-1.26	-8.85	-13.2	-16.1	-18.3
Diff kips	2.01	6.35	11.8	19.8	33.0	54.4	54.4	33.0	19.8	11.8	6.35	2.01
Note: λ and b are defined in Fig. 31.												

TABLE 11. CALCULATION OF V FOR HALF-SNOW LOADING

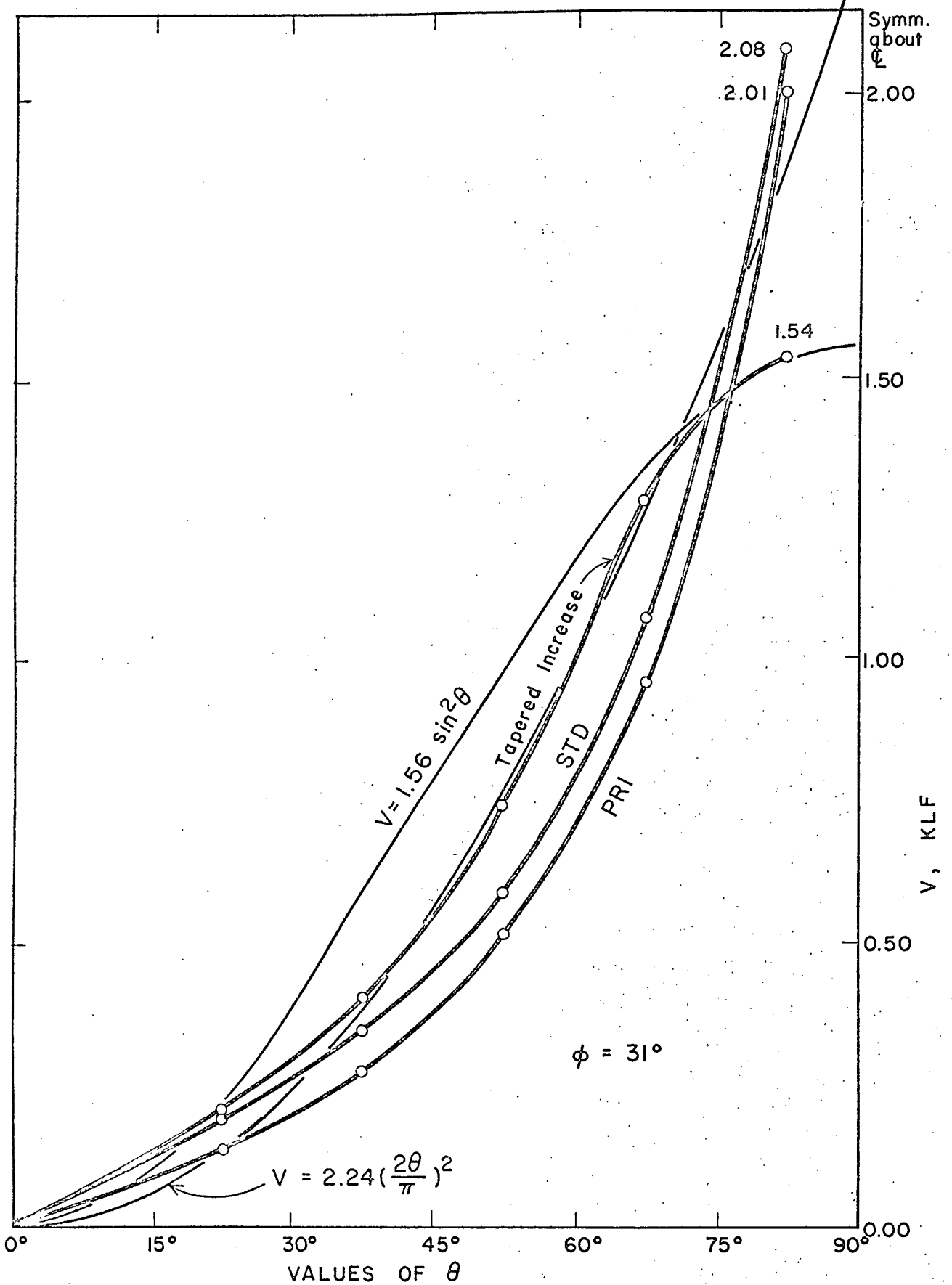

FIG. 30 V DISTRIBUTIONS FOR HALF SNOW

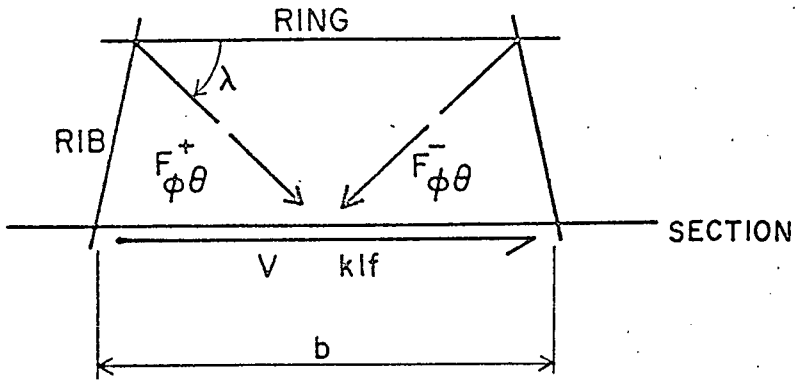

$$V = \left(F^{+}_{\phi\theta} - F^{-}_{\phi\theta} \right) \frac{\cos\lambda}{b} \quad \text{kIf}$$

FIG. 31 CALCULATION OF EXACT V

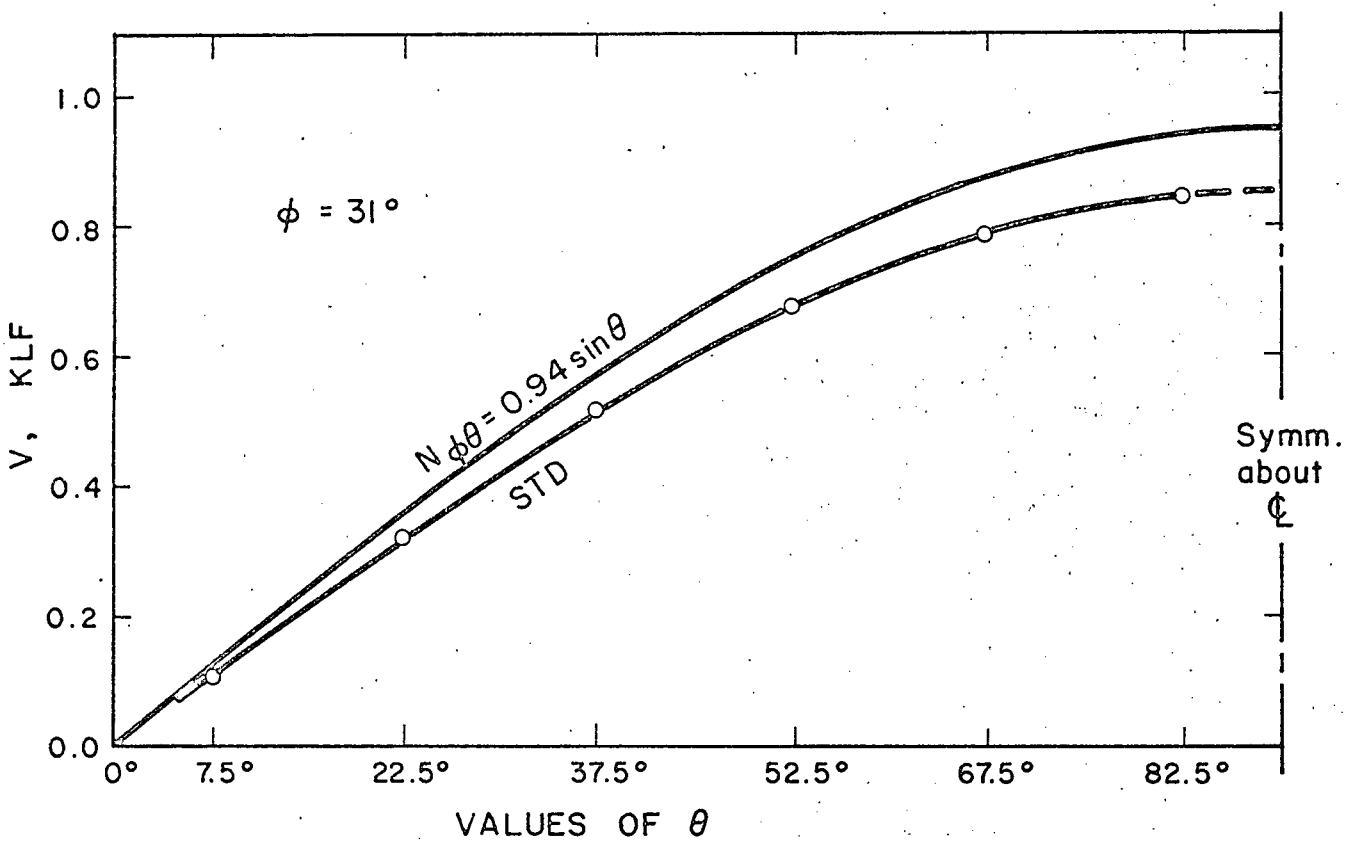

FIG. 32 V DISTRIBUTIONS FOR WIND

As a numerical example, for $\phi = 31^\circ$ and using the same values as for half snow, $V_o = 1.56$ klf and $V = 1.56 \sin^2\theta$ klf.

Comparison of this approximating distribution with the "Tapered Increase" curve of Fig. 30 is extremely good, the error being less than 1% at $\theta = 82.5^\circ$ which is the point of prime interest.

The shear flow V has been estimated fairly well by the approaches taken, but the problem remains to estimate $F_{\phi\theta}$ from V. At $\theta = 82.5^\circ$ and 97.5°, pairs of diagonals intersect and it was at these locations that the exact V was expected to be at a maximum. This was confirmed by the exact analysis.

For the standard dome subjected to half-snow loading, the approximation of V at $\theta = 82.5^\circ$ is:

$$V = 2.24 \left(\frac{2\theta}{\pi}\right)^2 = \frac{8.96}{\pi^2}\left(\frac{11\pi}{24}\right)^2 = 1.88 \text{ klf at } \phi = 31^\circ.$$

At this value of ϕ, b = 24.4 ft, $\cos\lambda = 0.853$,

hence $$F^+_{\phi\theta} - F^-_{\phi\theta} = \frac{bV}{\cos\lambda} = 53.8 \text{ kips}$$

according to Fig. 31.

Assuming $F^+_{\phi\theta}$ and $F^-_{\phi\theta}$ to be equal in magnitude, $F^+_{\phi\theta}$ will be 26.9 kips while $F^-_{\phi\theta}$ will be -26.9 kips. Table 11, which is the exact analysis of the standard dome for half snow, shows that the maximum value of $F^-_{\phi\theta}$ is 34.3 kips at $\phi = 31^\circ$ and $\theta = 97.5^\circ$. The ratio of actual/estimated is 1.28. The discrepancy is caused mainly by rib shortening due to F_ϕ which induces additional $F_{\phi\theta}$ forces. It may be concluded that the approximation for half snow is reasonable.

Considering next the results of the "Tapered Increase" snow load, it was found that at $\phi = 31^\circ$ the worst diagonal force was $F^-_{\phi\theta} = -25.6$ kips at $\theta = 97.5^\circ$. The approximation at this θ is

$$V = 1.56 \sin^2 97.5^\circ = 1.56\ (0.991)^2 = 1.53 \text{ klf}.$$

From this value, as before, for $\phi = 31^{\circ}$,

$$F^{+}_{\phi\theta} - F^{-}_{\phi\theta} = \frac{bV}{\cos\lambda} = 43.8 \text{ kips.}$$

Assuming $F^{+}_{\phi\theta}$ and $F^{-}_{\phi\theta}$ to be equal in magnitude, $F^{+}_{\phi\theta}$ will be 21.9 kips while $F^{-}_{\phi\theta}$ will be -21.9 kips. The ratio of actual/estimated is 1.17. This approximation is considered to be reasonable, too.

Finally, considering the modified Schwedler formula, the maximum $F_{\phi\theta}$ force is 73 kips at $\phi = 31^{\circ}$, and is for the tension diagonal since the compression diagonal was considered to be ineffective. This value is 23% higher than the sum of 59.6 kips found in Table 11 for the exact half snow analysis. At $\phi = 26^{\circ}$, the value from the modified Schwedler formula is about 60 kips and this is 10% higher than the sum of 54.4 kips.

In summary, Table 12 is presented to show the relative values produced by the methods discussed. With these tabulated values, the designer may approximate the maximum diagonal force for half snow loading provided that the proposed dome is geometrically similar.

4.3 Wind Loading

4.3.1 Shell Analogy

To approximate the maximum diagonal force caused by wind loading it was assumed that V, as defined in Fig. 28, is approximately equal to $N_{\phi\theta}$ of shell theory. For the wind loading, $p = p_o \sin\phi \cos\theta$, of Fig. 2, Flügge[4] presents this solution for a spherical shell:

$$N_{\phi\theta} = \frac{p_o a}{3} \frac{(2 + \cos\phi)(1 - \cos\phi)}{(1 + \cos\phi)\sin\phi} \sin\theta$$

where $N_{\phi\theta}$ = shear force, force/ unit distance,

p_o = wind pressure, force/unit area, at $\phi = 90^{\circ}$,

a = spherical radius, distance.

In this study $p_o = 0.0364$ ksf and $a = 181.67$ ft

so that $N_{\phi\theta} = 0.94 \sin\theta$ klf at $\phi = 31^{\circ}$.

TABLE 12. COMPARISON OF MAXIMUM DIAGONAL FORCES (KIPS) AT $\theta = 97.5^{\circ}$ FOR HALF-SNOW LOADING

Snow Depth Transition	Schwedler	Modified Schwedler	Thesis Approximation	Exact Maximum
	One Effective Diagonal		Two Effective Diagonals	
$\phi = 31^{\circ}$				
Abrupt Step	< 146	73	$\pm$26.9	-34.3
Tapered Increase	--	--	$\pm$21.9	-25.6
$\phi = 26^{\circ}$				
Abrupt Step	< 120	60	$\pm$25.5	-39.9
Tapered Increase	--	--	$\pm$20.7	-33.5
$\phi = 21^{\circ}$				
Abrupt Step	< 90	45	$\pm$23.5	-37.0
Tapered Increase	--	--	$\pm$19.2	-34.2

TABLE 13. CALCULATION OF V FOR WIND LOADING AT $\phi = 31^{\circ}$

θ degrees	$F^{+}_{\phi\theta}$ kips	$F^{-}_{\phi\theta}$ kips	Diff kips	$\frac{\cos\lambda}{b}$	V klf
7.5	7.35	4.20	3.15	0.035	0.110
22.5	10.0	0.76	9.25		.323
37.5	12.0	-2.75	14.8		.516
52.5	13.2	-6.06	19.2		.673
67.5	13.4	-8.95	22.4		.782
82.5	12.8	-11.2	24.0		.840

Comparison of this distribution with the exact analysis of the standard dome, STD, is shown in Fig. 32. At $\theta = 90^{o}$, the exact analysis distribution has a value of 0.85 klf and for domes PR1 and PR2, the corresponding values were 0.82 klf and 0.86 klf respectively.

It is seen in Fig. 32 on page 53, that the assumed distribution overestimates the worst exact shear flow by 10%. Table 13 shows the exact force values which are anti-symmetrical in nature. From $N_{\phi\theta} = 0.94 \sin \theta$ klf, the maximum $F_{\phi\theta}$ was calculated to be $\pm$13.3 kips which is 4% greater than the exact 12.8 kips at $\theta = 82.5^{o}$. Note that at adjacent panels 13.3 kips is a very good estimate.

4.3.2 Freebody Approach

Another approximation to the maximum $F_{\phi\theta}$ is presented now for a wind distribution which is not as simple as that of Fig. 2. In this approximation, Q, the resultant of the wind load, acts through A of Fig. 33 because the pressure is assumed to act perpendicular to the roof surface. Again, V_{ϕ} and M_{ϕ} forces at the section line have been neglected so that some error can be expected.

Inspection of the exact curve of V indicates that the following distribution could predict the shear flow:

$$V = V_{o} \sin \theta$$

The summation for the resultant of V is

$$H = 4\int_{o}^{\pi/2} V \sin \theta \, r d\theta = 4rV_{o}\int_{o}^{\pi/2} \sin^{2} \theta \, d\theta = \pi r V_{o}$$

and for the summation of moments about 0

$$H = \frac{T\,(d+m)}{d}$$

where T is the horizontal component of Q, so that

$$V_{o} = \frac{T\,(d+m)}{\pi r d} \quad .$$

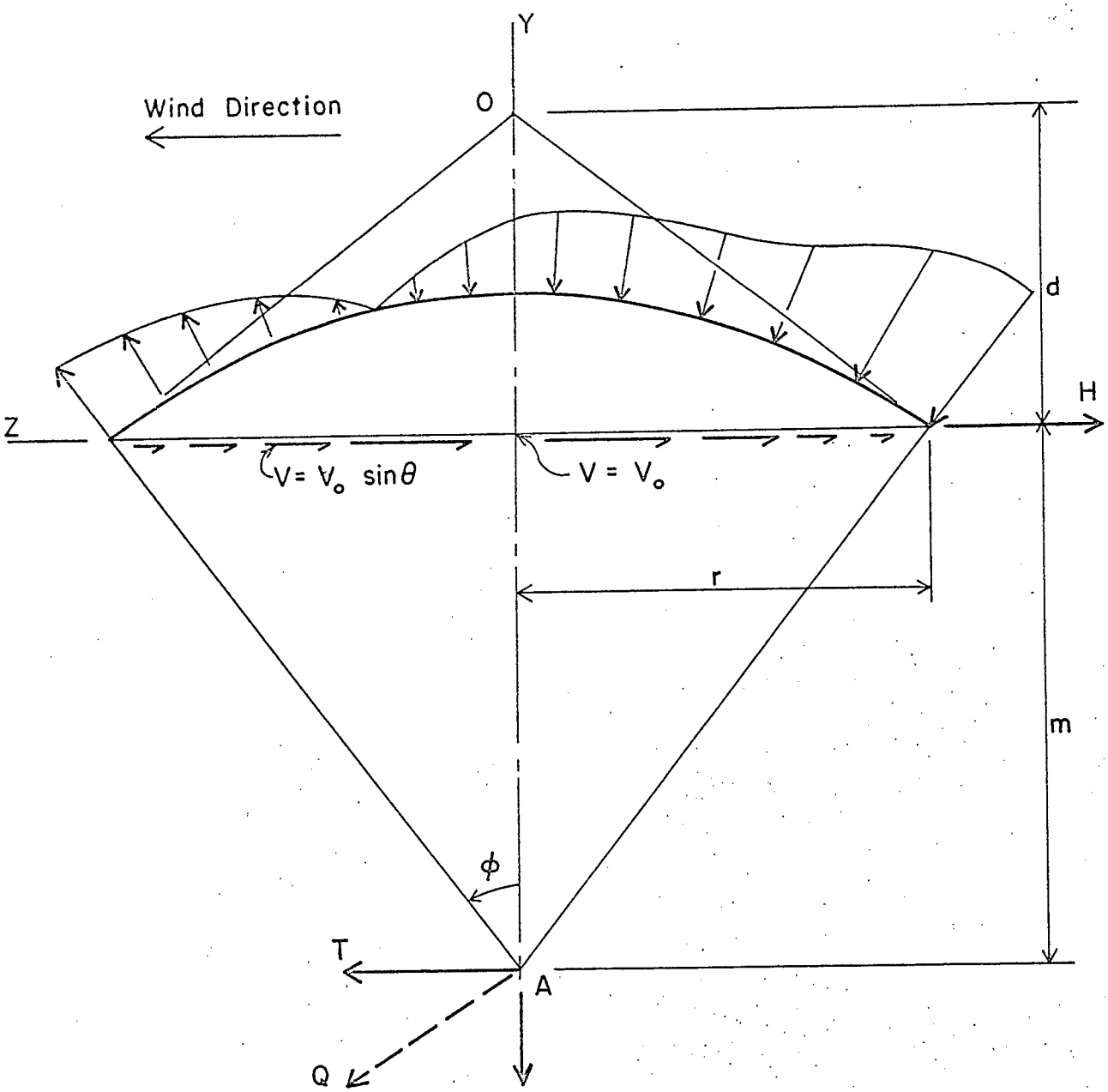

FIG. 33 FREEBODY FOR WIND

This expression for V_o is statically correct if the secondary forces V_ϕ and M_ϕ are neglected and depends on the assumption of a sine distribution of V.

As a numerical example, for the wind loading of Fig. 2,

$T = 73.4$ kips $\quad m = 155.7$ ft

$d = 56.2$ ft $\quad r = 93.6$ ft $\quad$ at $\phi = 31^o$,

from which $V_o = 0.94$ klf and $V = 0.94 \sin \theta$ klf. This coefficient is the same as that for $N_{\phi\theta}$ of shell theory because the assumptions for the $N_{\phi\theta}$ formula are equivalent to the omission of V_ϕ and M_ϕ forces.

It appears that a good approximation to $F_{\phi\theta}$ for wind, can be obtained either from shell theory or from the statics approach if a sine distribution of V is assumed.

CHAPTER V

CONCLUSIONS

A particular framed dome has been analyzed by an exact method based on six degrees of freedom per joint. The standard dome, as it was called, was found to be a reasonably designed structure for the loading conditions used for the study. It behaved in a predictable manner indicating that the structure stiffness matrix was well conditioned. However, this matrix was found to be sensitive when all of the members of the dome were pin-connected.

It has been stated in the past that a uniformly distributed load will control the design of the rib members and that unsymmetric loading will produce the maximum forces in diagonal members. This advice has been confirmed for the standard dome and its variations (except GEO).

The maximum rib forces were almost the same for full-snow and half-snow loading. However, if the dead load were included and a partial unbalance considered, as specified in many codes, then full loading definitely produces the maximum rib forces. The diagonal force induced by a uniformly distributed load and rib shortening is a fraction of that produced by unsymmetric loadings. Consequently, it can be stated that unsymmetric loads definitely govern the size of the diagonals. Whether wind or snow governs, will depend on the relative magnitude of these forces at specific geographic locations.

Although the ratio of bending/axial stress in the ribs approached five in some regions of the dome, the most highly stressed rib section used about one quarter of its strength to resist bending.

The effect of some parameter variations on the maximum member forces has been studied. For the wind and half-snow loadings used, reduction of the perimeter ring size increased both rib axial and rib bending moment forces, but decreased the web member forces. The unrealistic large reduction of web member area does create significant changes in member forces but since the variation in web member sizes in practice will be much smaller than that used herein, it can be concluded that reasonable alterations in web member sizes will not affect the member forces significantly.

Fixing all joints only reduced the deflection of the dome slightly. It should not be concluded from this that fixing of all joints is not important.

The study of a local dimple showed that a major increase in member forces near the depression occurred. Since the increase was large enough to cause failure of the members, steps should be taken to obtain a true shape during fabrication and erection.

Approximation methods for the maximum diagonal force have been tested for the unsymmetric loadings considered and found to be reasonable for preliminary analysis. More reliable data can be obtained from a computer analysis.

LIST OF REFERENCES

1 Schwedler, W., "Die Construction der Kuppeldächer", Zeitschr. f. Bauwesen, Jahrg. XVI, Bl. 12, 14, 1866.

2 Benjamin, B.S., "The Analysis of Braced Domes", Asia Publishing House, London, 1963.

3 Akademischen Verein 'Hütte', "Des Ingenieurs Taschenbuch", Abteilung II, Berlin, Wilhelm Ernst & Sohn, 1905.

4 Flügge, W., "Stresses in Shells", Springer-Verlag, Berlin, 1962.

APPENDIX

The following allowable stresses and design formulae are taken from CSA 086-1959, Code of Recommended Practice for Engineering Design in Timber, including revisions to February, 1961. The relevant clause number is shown at the right.

Allowable Unit Stresses (Elected) 3.3.1.1.

F_b = 2200 psi (bending stress)

F_c = 2070 psi (axial compression stress)

F_v = 190 psi (longitudinal shear stress)

E = 1800 ksi

Formulae for Simple Columns 1.6.2.2.

Definitions:

$\frac{\ell}{d}$ = slenderness ratio

$K = 0.641\sqrt{E/F_c}$

F_a = maximum allowable unit stress, psi

Short Column:

$$\ell/d \leq 10, \quad F_a = F_c$$

Intermediate Column:

$$10 < \ell/d \leq K, \quad F_a = F_c\left[1 - \frac{1}{3}\left(\frac{\ell/d}{K}\right)^4\right]$$

Long Column:

$$K < \ell/d \leq 50, \quad F_a = \frac{0.274\ E}{(\ell/d)^2}$$

Formula for Members Subjected to Combined Stress 1.6.4.

$$\frac{f_a}{F_a} + \frac{f_b}{F_b} \leqslant 1$$

where f_a = actual direct stress, psi,

F_a = maximum allowable unit stress in compression or tension, psi,

f_b = actual extreme fibre stress in bending, psi,

F_b = maximum allowable bending stress, psi.